Universidad de Concepción
Facultad de Ciencias Físicas y Matemáticas

Characterization of a Multiport Beam Splitter for High Dimensional Quantum Information Processing

Tesis para optar al grado de
Magíster en Ciencias con Mención en Física
por

Tania Andrea García Moscoso

September 8, 2020

Profesor Guía
Dr. Gustavo Lima Moreira

Agradecimientos

Quiero agradecer a mi familia que me apoyó desde la distancia, a mi pololo por su apoyo y por la paciencia que siempre me tuvo. A mis compañeros de laboratorio que siempre fueron muy simpáticos y amables conmigo, además de ensearme cómo funcionaba todo en el laboratorio, trataron de incorporarme desde el principio. A Gustavo Lima por darme la oportunidad de trabajar en su grupo de investigación, a mis otros profesores, y a Luciano, que siempre respondieron todas mis dudas de manera amable.

Esta tesis la dedico a mi madre Magdalena.

Abstract

A requirement for the implementation of quantum technologies is the ability to realize $N \times N$ unitary operators. It is essential for High dimensional quantum information processing (HD-QIP) tasks, which can outperform the two-dimensional ones. Nonetheless, the fabrication of such devices has been proven to be challenging, with progress only recently achieved with the advent of integrated photonics. Here, we report on the production of high-quality Multiport Beam Splitters (MBS), devices capable of performing $N \times N$ unitary operations, with $N = 4, 7$, over qudits, based on a new scheme for manipulating Multicore Fibers (MCF). We experimentally implemented a characterization protocol based on a practical interferometric method that requires only intensity measurements to directly determine the corresponding unitary matrices. Since the MBS were designed from multicore fibers, they present many advantages to overcome the challenges due to their practical and compact design. An important feature is that they can be used to build multi-arm interferometers, which when joined with other components allows one to implement efficient quantum circuits for HD-QIP. We also explored possible applications of these MBS by proposing the implementation of a positive operator valued mesurement (POVM), which are broadly relevant in many quantum information schemes, since they are able to distinguish probabilistically between nonorthogonal quantum states.

Resumen

Un requisito para la implementación de tecnologías cuánticas es la capacidad de realizar $N \times N$-operadores unitarios. Esto es esencial para las tareas de procesamiento de información cuántica en altas dimensiones (HD-QIP, por sus siglas en inglés), que pueden superar a las bidimensionales. No obstante, se ha demostrado que la fabricación de tales dispositivos es un desafío, con un progreso logrado sólo recientemente con el advenimiento de la fotónica integrada. Aquí, informamos sobre la producción de Divisores de Haz Multipuerto (MBS, por sus siglas en ingls) de alta calidad, dispositivos capaces de realizar $N \times N$-operaciones unitarias (con $N = 4, 7$), basados en un nuevo esquema para manipular Fibras Multi-núcleo (MCF, por sus siglas en inglés). Además, implementamos experimentalmente un protocolo de caracterización basado en un método interferométrico que requiere solo mediciones de intensidad para determinar directamente las matrices unitarias correspondientes. Dado que los MBS fueron diseñados a partir de MCF, presentan muchas ventajas para superar los desafíos debido a su diseño compacto. Una característica importante es que pueden usarse para construir interferómetros múlti-camino, que cuando se unen con otros componentes permiten implementar circuitos cuánticos eficientes para HD-QIP. También exploramos posibles aplicaciones de los MBS al proponer la implementación de una medición POVM (positive operator valued-measurement), ampliamente relevantes en muchos es-

quemas de información cuántica, ya que son capaces de distinguir probabilísticamente entre estados cuánticos no ortogonales.

Contents

List of Figures

List of Tables

Chapter 1

Introduction

In many schemes of quantum computation and quantum information, the experimental implementation of quantum technologies requires the ability to realize any $N \times N$ unitary operators, or quantum gates, to operate over quantum systems. Although it is known that any $N \times N$ unitary transformation can be produced by a standard method [1] using an arrangement of optical components, such as beam splitters, mirrors, and phase shifters, configuring and controlling these types of optical networks is still nontrivial. This is due to the fact that the schemes require a large number of standard 2×2-beam splitters when it comes to high dimensions. This is true even with decomposition methods [2] and more advanced arquitectures, such as photonic chips, where depending on the circuit size, the fidelity of the operations implemented can be compromised [3], [4].

Another practical challenge is the efficient characterization of these optical networks once they are built. Methods, such as quantum process tomography (QPT), using non-classical states or coherent states [5], and compressive sensing [6] have been large studied. Other approches require non-classical interference [7] or the use of an external interferometer [8]. However, for high dimensional networks, these approaches are relatively slow and impractical, in the case of QPT and

compressive sensing, and challenging, due to inteferometric stability requirements, in the other cases.

In this work, we introduce a high dimensional beam splitter, which is directly built within a multicore fiber employing a similar technique of [9], and propose an experimental method of characterization. The device is an example of a Multiport Beam Splitter, a physical device capable of implementing a $N \times N$ unitary operation over high dimensional quantum states, known as qudits. This operation is represented as a unitary matrix U, which transforms N input modes into N output modes. They also can be viewed as the generalization of the standard $N \times N$-beam splitter, a device that has been essential in many experiments of quantum information, and is described by a 2×2 unitary matrix that operates over two-level states, known as qubits.

The characterization is based on a technically practical interferometric method that requires only a laser source and intensity measurements to directly determine the unitary matrix. Based on the protocol of [10] we will be able to characterize a multiport without the need of an external interferometer or nonclassical interference.

Multicore fibers are specially designed optical fibers, in which several single-mode cores are physically contained within the same common cladding, with each core capable of transmitting data independently. They are employed by Space-division multiplexing (SMD) technology, that is considered to overcome the actual capacity limitation of optical telecommunication networks [11]. Since the Multiport Beam Splitters were designed from multicore fibers, they present many advantages to overcome the challenges due to their practical and compact design that allows a better control and high-fidelity propagation of qudits compared to the methods mentioned above. An important feature is that they can be used to build multi-arm interferometers, which when joined with other components (that can be

incorporated into the interferometer) allows one to implement efficient quantum circuits for HD-QIP on the prepare-measure scenarios [12].

We also, explored possible applications of this Multiport Beam Splitter by proposing the implementation of a POVM measurement, which are broadly relevant in many quantum information schemes, such us Quantum State Discrimination [13], Quantum Tomography [14], and Quantum Cryptography [15; 16]. Since the number of outcomes is not limited by the Hilbert space dimension of the measurement, they are able to distinguish probabilistically between nonorthogonal quantum states [17]. Due to the experimental challenges of implementating higher-dimensional non-projective measurements, realizations have been limited to qubit systems [18]. In this work, we will focus on the case of a four-dimensional non-projective measurement with seven outcomes.

1.1 Overview of the Thesis

In the Chapter 2 we present the mathematical framework used in this thesis, reviewing the foundations of quantum mechanics, showing in more detail the concept of general measurement and the advantages over projective measurements. In Chapter 3, we show the theory of linear multiports, from the beam splitter to the concept of multiport, and the different designs to build them. In Chapter 4 we describe the device in study, which is a multiport represented by a multicore fiber beam splitter of N cores, and the technique of fabrication. In Chapter 5 we explain the protocol of characterization of a multiport beam splitter that will be applied to characterize the device in study. Next, in Chapter 6, we showed the experimental setup and the measurement procedure, following the protocol. In Chapter 7 we present the results and analysis of this experimental work, and finaly, in the Chapter 8, we propose the implementation of a POVM measurement,

as a study of posible applications.

Chapter 2

Quantum Mechanics

Summary

Quantum Mechanics is a theory which allows us to describe the behavior of microscopic physical systems, such as atoms and photons. The quantum theory has deep differences with classical theories. The main one is the measurement process. Classical physics implicitly assumes the properties of systems to be unchanged by measurement processes. Thereby, different properties can be measured without any interference among them. This is not the case in quantum physics, where the measurements can have random outcomes and they disturb the state of the system. Thereby, the measurement of a property typically precludes the knowledge about other properties. Quantum Mechanics has allowed the development of many technological applications, such as Quantum Information, Quantum Computation and Quantum Cryptography.

2.1 Postulates of Quantum Mechanics

In this section, we review shortly all the postulates of quantum mechanics. There are four basic postulates which tell us how to describe all we can know about a quantum system [19].

2.1.1 State Space

The first postulate refers to the mathematical representation of quantum systems, using a mathematical object, which allows us to predict the result of all possible experiments on the system.

Postulate 1: *Any isolated physical system is associated with a complex vector space with inner product (called a Hilbert space $\mathcal{H}$) known as the state space of the system. The state vector is a unit vector in the systems state space and completely describes the system.*

A state vector $|\psi\rangle$ is a normalized vector in the Hilbert space, $|\langle\psi|\psi\rangle| = 1$, which can be identified also as an equivalence class, then $|\psi\rangle$ is defines the same physical state as $e^{i\varphi}|\psi\rangle$. The simplest quantum mechanical system is the *qubit (quantum bit)*[1], a 2-dimensional quantum system. Which can be written as the following general form

$$|\psi\rangle = \alpha|0\rangle + \beta|1\rangle \ , \tag{2.1}$$

where $\{|0\rangle, |1\rangle\}$ is the orthonormal basis of that state space, and α and β are complex numbers, which satisfy the unitary condition $|\alpha|^2 + |\beta|^2 = 1$. In general, a d dimensional state is called a *qudit (quantum dit)*.

An alternative formulation is possible using a tool known as the *density operator*

[1] Inspired by the bit notion of classical computing.

or *density matrix*.The language of density matrices is convenient for describing systems that are not fully known. This is a system that can't be described only with a state $|\psi\rangle$, instead we need a set of n states $|\psi_i\rangle$ with their respective probabilities p_i, called the *ensemble of pure states* $\{p_i, |\psi_i\rangle\}_{i=1,\ldots,n}$. The density operator of the system is defined by the equation

$$\rho = \sum_{i=1}^{n} p_i |\psi_i\rangle\langle\psi_i|. \tag{2.2}$$

Note that the expansion (2.2) does not necessarily coincide with the spectral decomposition of ρ and n can be different than $\dim(\mathcal{H})$. The density operators are characterized by the following theorem:

Teorema 1.- *An operator ρ is a density operator associated to some ensemble $\{p_i, |\psi_i\rangle\}_{i=1,\ldots,n}$ if and only if it satisfies the conditions:*

1. The trace of ρ is equal to 1. That is, $\mathrm{Tr}(\rho)= 1$,

2. $\rho \in \mathcal{P}$. That is, ρ is positive semidefinite operator.

Density matrices are classified into two types: if there exists a vector $|\psi\rangle$ such that $\rho = |\psi\rangle\langle\psi|$, then we say that the state is pure; otherwise we say that the state is mixed. A state ρ can be determined as pure or mixed by evaluating its *purity*, $\mathrm{Tr}(\rho^2)$, being completely pure when $\mathrm{Tr}(\rho^2) = 1$.

2.1.2 Evolution

The second postulate describes how evolve a closed quantum system, which is a system that does not interact with any other systems.

Postulate 2: *The evolution of a closed quantum system is described by a unitary transformation. That is, if a state in an initial time t_0 is $|\psi\rangle$, and in a final time t it is $|\psi'\rangle$, then the relationship between these two states is given by an*

unitary operator $U(t_0, t)$. This relation is written as:

$$|\psi(t)\rangle = U(t, t_0)|\psi(t_0)\rangle. \tag{2.3}$$

We can calculate the evolution of a density operator,

$$\rho(t) = \sum_{i=1}^{n} p_i |\psi_i(t)\rangle\langle\psi_i(t)| \tag{2.4}$$

$$= \sum_{i=1}^{n} p_i U(t, t_0)|\psi_i(t_0)\rangle\langle\psi_i(t_0)|U(t, t_0)^\dagger \tag{2.5}$$

$$= U(t, t_0)\left(\sum_{i=1}^{n} p_i |\psi_i(t_0)\rangle\langle\psi_i(t_0)|\right) U(t, t_0)^\dagger \tag{2.6}$$

$$= U(t, t_0)\rho(t_0)U(t, t_0)^\dagger. \tag{2.7}$$

Furthermore, the general evolution of a density matrix is a completely positive map that preserves the trace, which can be represented by a set of $n \leq d^2$ operators $\{K_i\}_{i=1,\ldots,n}$ which satisfies $\sum_{i=1}^{n} K_i^\dagger K_i = \mathbb{I}$, called *Kraus Operators* [19],

$$\rho(t) = \sum_{i=1}^{n} K_i \rho(t_0) K_i^\dagger. \tag{2.8}$$

A system can evolve into another (mixed) system through interactions with a second system that is not described by ρ. Eq. (2.8) allows one to describe this type of evolution.

2.1.3 Quantum Measurements

According to Postulate 2 of quantum mechanics, it is well known that closed, isolated, quantum systems, where there is no interaction between the system and

the environment, evolve according to unitary evolution. However, real quantum systems are not closed, this interaction always occurs, either because of the existence of noise or environmental disturbances or because of the interaction with the measuring device. For example, when the experimentalists and their experimental equipment, an external physical system, observe the system to discover what is going on inside the system, an interaction that makes the system no longer closed, and thus not necessarily subject to unitary evolution.

Postulate 3: *The quantum measurement is described by a collection* $\{M_m\}$ *of measurement operators, which act on the Hilbert space of the system being measured. The index* m *refers to the measurement outcomes that may occur in the experiment. These measurement operators satisfy the completness equation,*

$$\sum_m M_m^\dagger M_m = I \tag{2.9}$$

This equation expresses the fact that probabilities sum to one. If the system is in a state $|\psi\rangle$*, immediately before the measurement then the probability of the outcome* m*, asociated with* M_m*, is given by:*

$$p(m) = \langle\psi|M_m^\dagger M_m|\psi\rangle \tag{2.10}$$

and the state of the system after the meaurement is

$$\frac{M|\psi\rangle}{\sqrt{\langle\psi|M_m^\dagger M_m|\psi\rangle}} \,. \tag{2.11}$$

For a density matrix and a measurement $\{M_m\}_{m=1,\ldots,n}$ on the ensemble $\{p_i, |\psi_i\rangle\}_{i=1,\ldots,n'}$ we have that the probability of obtaining outcome m is

$$p(m) = \sum_{i=1}^{n'} p(m|i)p_i \tag{2.12}$$

$$= \sum_{i=1}^{n'} \langle\psi_i|M_m^\dagger M_m|\psi_i\rangle p_i \tag{2.13}$$

$$= \sum_{i=1}^{n'} \mathrm{Tr}(M_m^\dagger M_m|\psi_i\rangle\langle\psi_i|)p_i \tag{2.14}$$

$$= \mathrm{Tr}(M_m^\dagger M_m \sum_{i=1}^{n'} p_i|\psi_i\rangle\langle\psi_i|) \tag{2.15}$$

$$= \mathrm{Tr}(M_m^\dagger M_m \rho), \tag{2.16}$$

where $p(m|i)$ is the conditional probability of m if the initial state was $|\psi_i\rangle$. The states of the ensemble after the measurement are

$$|\psi_i^m\rangle = \frac{M_m|\psi_i\rangle}{\sqrt{\langle\psi_i|M_m^\dagger M_m|\psi_i\rangle}}. \tag{2.17}$$

with respective probabilities $p(i|m)$. Then, the density matrix after the measurement is

$$\rho^m = \frac{M_m \rho M_m^\dagger}{\mathrm{Tr}(M_m^\dagger M_m \rho)}. \tag{2.18}$$

2.1.4 The problem of distinguishing quantum states

An important measurement scenario is the ability to distinguish quantum states. In principle, it is possible to distinguish the states of an object in the classical world, as easy as identifying the face of a landed die that was rolled. However, things aren't straightforward in the quantum world, the difficulty of distinguishability depends on the orthogonality of the set of quantum states. In section 2.2.4 of the book [20], it is shown that non-orthogonal quantum states cannot be dis-

tinguished, unlike orthogonal states. To understand and analyze this problem, it is useful to consider two cases of measurements, projective measurements and POVMs.

2.1.5 Projective measurement

When operators satisfy the conditions that they are orthogonal projectors, that is, the M_m are hermitian and $M_m M_{m'} = \delta_{m,m'} M_m$, the measurement is said to be projective measurement. This special case of measurement is described by an observable, M, a Hermitian operator on the state space of the system being observed. The observable has a spectral decomposition,

$$M = \sum_m m P_m \ , \tag{2.19}$$

where $P_m = M_m$ is the projector onto the eigenspace of M with eigenvalue m. Then the completness relation can be written as follows

$$\sum_m P_m = I \ . \tag{2.20}$$

If the initial state is $|\psi\rangle$, then the probability of getting the result m is

$$p(m) = \langle \psi | P_m | \psi \rangle \tag{2.21}$$

and the state after measurement,

$$\frac{P_m |\psi\rangle}{\sqrt{p(m)}} \tag{2.22}$$

2.1.6 POVM measurements

As a consequence of the general description of measurements, the POVM formalism, which acronym stands for 'Positive Operator-Valued Measure', is suitable for instances where the system can be measured only once, at the end of the experiment, for example photon measurement.

In this case is usually to define $E_m = M_m^\dagger M_m$ as positive operators such that, $\sum_m E_m = I$ and $p(m) = \langle\psi|E_m|\psi\rangle$. The operators E_m are known as the POVM elements associated with the measurement. The complete set of $\{E_m\}$ is known as a POVM, and is sufficient to determine the probabilities of the different measurement outcomes.

2.1.7 Composite Systems

Composite quantum systems are formed by two or more subsystems. The following postulate describes how the state space of a composite system is built up from the state spaces of the component systems.

Postulado 4: *The state space of a composite physical system is the tensor product of the state spaces of the component physical systems. If the subsystems are numbered from* 1 *to* n*, the state space is*

$$\mathcal{H} = \mathcal{H}_1 \otimes \mathcal{H}_2 \otimes ... \otimes \mathcal{H}_n. \tag{2.23}$$

In particular, if the subsystems are prepared in the states $\{|\psi_i\rangle\}_{i=1,...,n}$, the state of the system is

$$|\Psi\rangle = |\psi_1\rangle \otimes |\psi_2\rangle \otimes ... \otimes |\psi_n\rangle. \tag{2.24}$$

It is important to remark that not all states in the composite space are of this form. If a state can be written in the form (2.24) we call it *separable*. Otherwise, we say it is *entangled*. Let us consider the two qubit space, which is a 4-dimensional Hilbert space. A separable basis of this space is

$$|00\rangle = |0\rangle \otimes |0\rangle \quad |01\rangle = |0\rangle \otimes |1\rangle \quad |10\rangle = |1\rangle \otimes |0\rangle \quad |11\rangle = |1\rangle \otimes |1\rangle. \tag{2.25}$$

On the other hand, an entangled basis is the *Bell Basis*,

$$|\psi^{\pm}\rangle = \frac{1}{\sqrt{2}} \left(|01\rangle \pm |10\rangle\right) \qquad |\phi^{\pm}\rangle = \frac{1}{\sqrt{2}} \left(|00\rangle \pm |11\rangle\right). \tag{2.26}$$

The entangled states are used in Quantum Teleportation [21], Quantum Cryptography [22] and fundamental tests of Quantum Mechanics [23].

Chapter 3

Theory of $N \times N$ Beam Splitters

Summary

In this chapter we explain the theory needed to comprehence the concept of Multiport Beam Splitters, and the most well-known designs to construct them. We started from the concept of the very known standard beam splitter (the 2×2 Beam Splitter), to continue with its generalization, a Multiport Beam Splitter (which is a $N \times N$ Beam Splitter, when $N > 2$).

3.1 The 2×2 Beam Splitter

A 2×2 Beam splitter is a physical device used in experiments of quantum optics to operates over two-level quantum systems, qubits. Formally, for a given state $|\psi_0\rangle$ in a 2-dimensional Hilbert space the transformation into another vector $|\psi_1\rangle$ is represented by a unitary matrix U. This transformation can be realized with a beam splitter whose matrix transforms the input state with modes (k_1, k_2) into the output state with modes (k_1', k_2'). We will use the following representation of the beam splitter matrix:

$$\begin{pmatrix} k_1' \\ k_2' \end{pmatrix} = \begin{pmatrix} \sin\omega & e^{i\phi}\cos\omega \\ \cos\omega & -e^{i\phi}\sin\omega \end{pmatrix} \begin{pmatrix} k_1 \\ k_2 \end{pmatrix} ,$$

where ω describes the reflectivity and transmittance of the beam splitter, and ϕ describes the relative phase between the input modes. It can be modified utilizing an external phase shifter before the beam splitter.

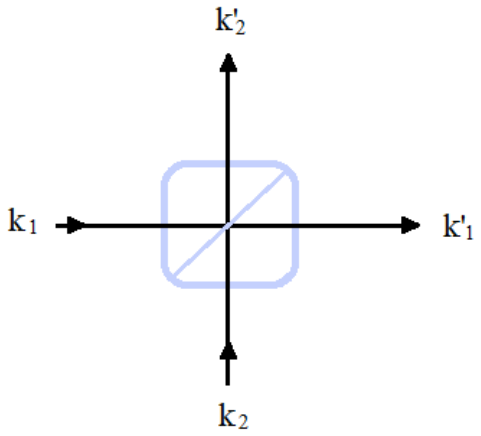

Figure 3.1: Beam Splitter scheme. The BS transform de input modes (k_1, k_2) into the output modes (k_1', k_2').

The use of external phase shifters after the BS output ports allows the beam splitter matrix to perform any transformation in U(2) [24; 25]. On the other hand, a beam splitter with variable reflectivity can be substituted by a Mach-Zhender interferometer using two symmetric 50:50 beam splitters.

3.2 The Multiport Beam Splitter

A Multiport Beam Splitter is a physical device that can be used in experiments of quantum information to operates over N-level quantum systems, qudits, with $N > 2$. They can be viewed as the generalization the standar beam splitter, that

we mentioned previously. For a given state $|\psi_0\rangle$ in a N-dimensional Hilbert space the transformation into another vector $|\psi_1\rangle$ is represented by a unitary matrix U. Experimentally, this transformation can be realized with a multiport beam splitter whose matrix transforms N input modes into N output modes. We will use the following representation:

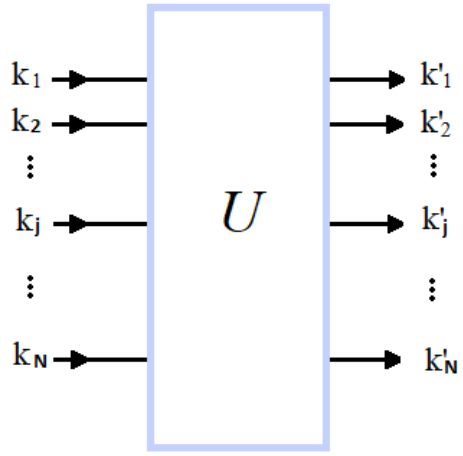

Figure 3.2: Multiport Beam Splitter scheme represented by the unitary matrix U. It transforms de input modes $(k_1, k_2, ..., k_N)$ into the output modes $(k'_1, k'_2..., k'_2)$.

A usual method to construct an MBS is the one proposed by M. Reck et al in 1994 [1], in which an specific triangular mesh of interconnected standard 2×2-beam splitters and phase shifters were enough to produce experimentally a unitary transformation $N \times N$ in the laboratory. They established that in any optical experiment representing a unitary matrix, it can be decomposed into a product of blocks $T_{m,n}$ containing only beam splitter matrices with appropriate phase shifts. More recently, in 2017, Clements et al [2] proposed a designed based on the Reck's, using the same number of beam splitters, but with a square geometry, and giving shorter optical depth [1], and therefore, providing a design that is more symmetric

[1]The longest path through the interferometer, enumerated by counting the number of beam splitters traversed by that path.

and robust than Reck configuration. The minimal number of 2×2 beam splitters needed to implement an N-dimensional unitary matrix is $N(N-1)/2$, the same for both cases. For example, we will need thirty-six beam splitters for the $N = 9$ dimension, both designs are shown in Fig. 3.3. Other designs have been obtained, which even require fewer beamsplitters compared to the Reck and Clements designs [26; 27; 28]. However, all those configurations are not able to implement an arbitrary unitary operator, unlike Reck's method.

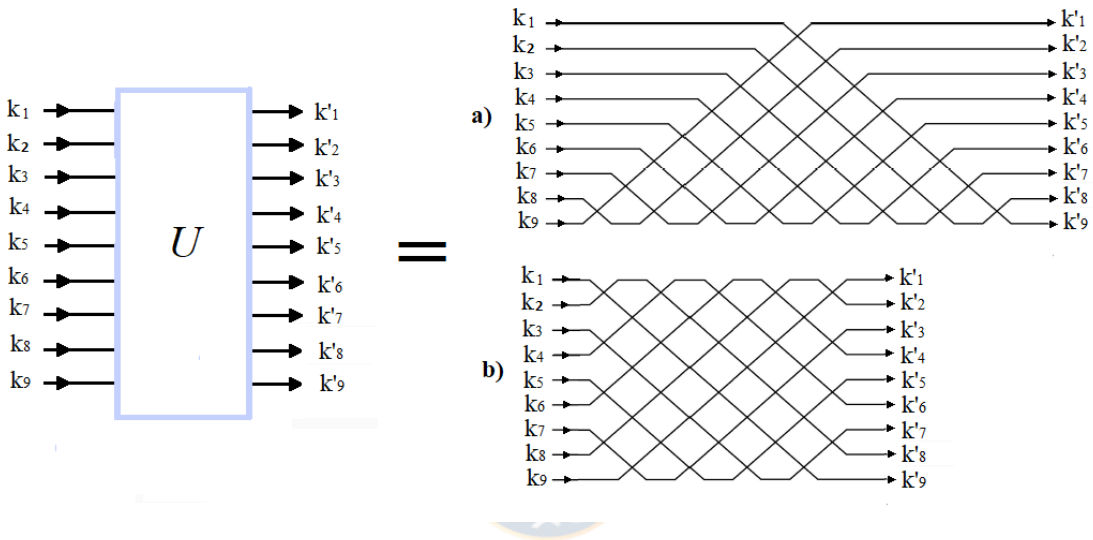

Figure 3.3: Designs to contruct a Unitary Operator with dimension $N = 9$. In the left, the Multiport Beam Splitter. In the right, a) Reck design and b) Clements design. Both, a) and b), use the same number of beam splitters, $N(N-1)/2 = 36$.

The multiport beam splitter is an important unitary transformation. Being a high dimensional beam splitter (a type of "super beam splitter"), it allows to implement reconfigurable multi-path interferometers and, consequently, a variety of $N \times N$ unitary operations.

Chapter 4

Multicore Fiber Multiport Beam Splitters

Summary

In this chapter we introduce and describe the device studied in this thesis, from its fabrication to the potential use it has in quantum information experiments.

4.1 Multicore fibers

Space-division multiplexing (SDM) is currently the main technology considered to overcome the actual capacity limitation of optical telecommunication networks [11]. Basically, it consists of specially designed fibers that can support distinct spatial optical modes in order to increase the multiplexing capabilities. The optical fibers employed by SDM can be devided into two main groups: multicore fibers (MCF) [29] and few-mode fibers (FMF)[30; 31]. In the former, several single-mode cores are physically contained within the same common cladding, with each core being used independently. A few-mode fiber on the other hand consists of a single

core that supports several optical modes, each of them capable of transmitting data independently. Arguably, the development of a major part of experimental quantum information (QI) relies on the fact that it is heavily based on the same hardware eployed by classical optical communication [32; 33]. Therefore, it is natural to expect that future development will take place using SDM hardware [34]. Indeed, in the past couple of years the first quantum communication (QC) experiments based on MCF have appeared. The first one used a MCF as a direct multiplexing device: with one core acting as the quantum channel, while other cores contained classical data [35]. See also refs [36; 37]. Later, the fact that all cores are placed in a common cladding translates to a long multipath conduit with intrinsic phase stability, was explored for demonstrating the feasibility of high-dimensional quantum key distribution (HD-QKD) over MCFs [38; 39].

The benefit of MCFs for QI has been further reinforced by showing that they can support propagation of entangled photons [40; 41]. Similar research has begun for few-mode fibers (FMFs) [42; 43; 44; 45; 46]. Additionally, SDM technology has been exploited for building optical fiber sensors based on MCFs, whose remote interrogation makes them attractive for industrial applications [9; 47; 48; 49]. MCF optical sensors have been used for high-temperature sensing up to 1000 C with a typical temperature sensitivity as high as 170 pm/C [49]. The advantage of using MCFs is that they allow for the fabrication of multi-arm Mach-Zehnder (MZ) interferometers, that have higher sensitivity for phase changes since the slopes of the resulting interference peaks are steeper. There has been a large variety of MCF optical sensors but most of them rely on inefficient techniques to launch light into a multi-arm interferometer, resulting in prohibitive losses for quantum information processing. Of particular interest is the work of L. Gan et. al. [9], where the authors develop new tapering techniques to build the multi-arm interferometer directly into a specially designed MCF.

4.2 Fabrication of a Multiport Beam Splitter using a Multicore Fiber

As mentioned before, multicore fibers can be exploited for the propagation of path qudit states defined as the coherent superposition [38],

$$|\psi\rangle = \frac{1}{\sqrt{k}} \sum_{0}^{k} e^{i\phi_k} |k\rangle \ , \tag{4.1}$$

where $|k\rangle$ denotes the state of the photon transmitted by the kth core mode, and ϕ_k is the relative phase acquired during propagation over the kth core (see Fig. 4.1 a). However, to produce such a state and to measure it requires efficient coupling of light into all of the $k+1$ cores of the MCF. This is the important role of the MCF-based MBS. Following a recent tapering technique introduced in [9] we could be able to construct high-quality 4×4 and 7×7 multiport beam splitters. In that work, the authors were interested in building multi-arm Mach Zehnder interferometers for multiparameter estimation. Their idea was to use an heterogeneous multicore fiber that is used to minimise inter-core coupling, as it has lower refractive-index "trenches" around the cores. In such fibers, there are two orthogonal modes propagating over one core of the fiber, which normally never interfere. Nonetheless, by tapering this fiber, they created an overlap between such modes due to strong evanescence effects in the tapered zone. From the interference observed, parameter estimation was possible. The author then used each core interference for estimating different parameters of a sample. The fiber worked as an instrument composed of several 2-path MZ interferometers. In their tapered region, the inter-coupling between different cores was severely reduced by such trenches.

Here, we show that by employing the same technique but with homogeneous

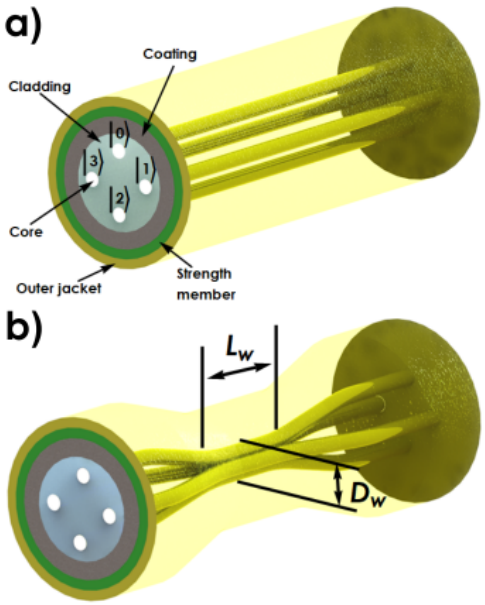

Figure 4.1: Schematics of a MCF and of the fabricated MBSs of 4 cores. a) MCF before tapering and the qudit encoding strategy. b) The fiber is then heated along a length L and pulled symmetrically from both ends, streching and thinning the fiber. The final device is the MBS and has a length L_W with dimameter D_W.

MCFs, i.e., fibers where the N cores are not bounded by refractive index trenches, one can build high-quality Multiport Beam Splitters ($N \times N$ beam splitters). The tapering is performed by locally heating a small transverse region of the fiber with length L, while applying a controlled longitudinal stretching tension. Since the fiber is mechanically in a partial soft state, it will become thinner with a final diameter D_w at the center of the region where the heat is applied. The cores will consequently be brought together, and due to evanescent coupling, light will leak from one core to the others, similar to what is obtained in a standard fiber-optical bi-directional coupler (See Fig. 4.1 b). Due to the symmetry of the 4-core MCF structure, the splitting ratio can be balanced for all core-to-core combinations. Finally, since the Multiport Beam Splitter is directly constructed on a MCF, it is compatible for connection with other MCFs by direct contact (i.e. FC/PC fiber

connectors).

Chapter 5

Characterization of a Multiport Beam Splitter

Summary

In this section we review the procedure used to characterize a unitary Multiport Beam Splitter (MBS). We start from the most general form of a unitary matrix representing a MBS, which is used for obtaining the amplitudes and relative phases, to end with an optimization method to solve the problem of the non-unitary matrix that appears due to experimental errors.

5.1 Unitary matrices

A unitary matrix U is a complex square matrix whose inverse is equal to its conjugate transpose, that is $UU^\dagger = U^\dagger U = I$. They have significant importance in quantum mechanics because they preserve norms, and thus, probability amplitudes. The following properties hold for a finite size unitary matrix:

- U preserves the inner product.

- U is normal.
- U is diagonalizable
- $|\det(U)| = 1$
- Its eigenvectors corresponding to different eigenvalues are orthogonal.
- U can be written as $U = e^{iH}$, with H a Hermitian matrix.

As a consequence of unitarity it is easy to see that columns (and similarly rows) of U form a complex orthonormal basis. The unitary matrices of size $d \times d$ form a group called unitary group $U(d)$, with the group operation of matrix multiplication. Each element of this group is characterized by d^2 real parameters. A general exppression for U is:

$$U = \begin{pmatrix} u_{11}e^{i\phi_{11}} & u_{12}e^{i\phi_{12}} & \cdots & u_{1d}e^{i\phi_{1d}} \\ u_{21}e^{i\phi_{21}} & u_{22}e^{i\phi_{22}} & \cdots & u_{2d}e^{i\phi_{2d}} \\ \vdots & \vdots & \ddots & \vdots \\ u_{d1}e^{i\phi_{d1}} & u_{d2}e^{i\phi_{d2}} & \cdots & u_{dd}e^{i\phi_{dd}} \end{pmatrix} \tag{5.1}$$

where u_{ij} and ϕ_{ij} are real numbers. An important subgroup of $U(d)$ is the special unitary group $SU(d)$, whose elements have determinat 1. Thus, they are characterized only by $d^2 - 1$ real parameters.

Let us define a real-border unitary matrix as a unitary one, such that, its first row and column are real and positive,

$$V = \begin{pmatrix} v_{11} & v_{12} & \cdots & v_{1d} \\ v_{21} & v_{22}e^{i\varphi_{22}} & \cdots & v_{2d}e^{i\varphi_{2d}} \\ \vdots & \vdots & \ddots & \vdots \\ v_{d1} & v_{d2}e^{i\varphi_{d2}} & \cdots & v_{dd}e^{i\varphi_{dd}} \end{pmatrix} \tag{5.2}$$

where $v_{jk} \geq 0$. Clearly, one can transform an arbitrary unitary matrix U to a real-border unitary matrix V, by multiplying it by diagonal matrices with $2d-1$ phases of the first columns and rows. Thus, one could think that the real-border unitary matrices are characterized only by $d(d-2)$ parameters. However, it has been shown that this is not true for dimensions greater than 3 [50]. Usually, multiport beam splitters are characterized by unitary transformations with real border, since the phases of the border often can not be experimentally determined. Therefore, the family of unitary transformations that can be implemented by a fixed real-border multiport beam splitter V and phase shifters are:

$$U = \begin{pmatrix} e^{i\phi_{11}} & & & \\ & e^{i\phi_{21}} & & \\ & & \ddots & \\ & & & e^{i\phi_{d1}} \end{pmatrix} V \begin{pmatrix} 1 & & & \\ & e^{i(\phi_{12}-\phi_{11})} & & \\ & & \ddots & \\ & & & e^{i(\phi_{1d}-\phi_{11})} \end{pmatrix} \tag{5.3}$$

A multiport beam splitter is called symmeric if the norm of all its matrix elements are equal,

$$v_{nm} = \frac{1}{\sqrt{d}} \, . \tag{5.4}$$

Thereby, a symmetric real-border multiport beam splitter reads

$$W = \frac{1}{\sqrt{d}} \begin{pmatrix} 1 & 1 & \cdots & 1 \\ 1 & e^{i\varphi_{22}} & \cdots & e^{i\varphi_{2d}} \\ \vdots & \vdots & \ddots & \vdots \\ 1 & e^{i\varphi_{d2}} & \cdots & e^{i\varphi_{dd}} \end{pmatrix} \, . \tag{5.5}$$

The most known symmetric multiport beam splitters are the canonical one, whose

matrix elements are given by

$$F_{nm}^{(d)} = \frac{1}{\sqrt{d}} e^{2\pi i(n-1)(m-1)/d} \,. \tag{5.6}$$

For example, for $d = 2$ we have the Hadamard matrix,

$$F^{(2)} = \frac{1}{\sqrt{2}} \begin{bmatrix} 1 & 1 \\ 1 & -1 \end{bmatrix} \,. \tag{5.7}$$

For $d = 4$ we have

$$F^{(4)} = \frac{1}{2} \begin{bmatrix} 1 & 1 & 1 & 1 \\ 1 & i & -1 & -i \\ 1 & -1 & 1 & -1 \\ 1 & -i & -1 & i \end{bmatrix} \,, \tag{5.8}$$

and for $d = 7$ the canonical multiport beam splitter is

$$F^{(7)} = \frac{1}{\sqrt{7}} \begin{bmatrix} 1 & 1 & 1 & 1 & 1 & 1 & 1 \\ 1 & e^{\frac{2\pi}{7}i} & e^{\frac{4\pi}{7}i} & e^{\frac{6\pi}{7}i} & e^{\frac{8\pi}{7}i} & e^{\frac{10\pi}{7}i} & e^{\frac{12\pi}{7}i} \\ 1 & e^{\frac{4\pi}{7}i} & e^{\frac{8\pi}{7}i} & e^{\frac{12\pi}{7}i} & e^{\frac{2\pi}{7}i} & e^{\frac{6\pi}{7}i} & e^{\frac{10\pi}{7}i} \\ 1 & e^{\frac{6\pi}{7}i} & e^{\frac{12\pi}{7}i} & e^{\frac{4\pi}{7}i} & e^{\frac{10\pi}{7}i} & e^{\frac{2\pi}{7}i} & e^{\frac{8\pi}{7}i} \\ 1 & e^{\frac{8\pi}{7}i} & e^{\frac{2\pi}{7}i} & e^{\frac{10\pi}{7}i} & e^{\frac{4\pi}{7}i} & e^{\frac{12\pi}{7}i} & e^{\frac{6\pi}{7}i} \\ 1 & e^{\frac{10\pi}{7}i} & e^{\frac{6\pi}{7}i} & e^{\frac{2\pi}{7}i} & e^{\frac{12\pi}{7}i} & e^{\frac{8\pi}{7}i} & e^{\frac{4\pi}{7}i} \\ 1 & e^{\frac{12\pi}{7}i} & e^{\frac{10\pi}{7}i} & e^{\frac{8\pi}{7}i} & e^{\frac{6\pi}{7}i} & e^{\frac{4\pi}{7}i} & e^{\frac{2\pi}{7}i} \end{bmatrix} \,. \tag{5.9}$$

For factorizable dimensions, symmetric multiport beam splitters can be constructed by the tensor product of symmetric multiport beam splitters of size equal to its prime factors. In general, the number of parameters that characterize a symmetric multiport beam splitter is not known. Neverthless, the parametric family of

this type of multiports are known for factorizable dimensions. For example, the parametric family of symmetric multiport beam splitters on dimension 4 are:

$$V = \frac{1}{2}\begin{bmatrix} 1 & 1 & 1 & 1 \\ 1 & e^{i\phi} & -1 & -e^{i\phi} \\ 1 & -1 & 1 & -1 \\ 1 & -e^{i\phi} & -1 & e^{i\phi} \end{bmatrix} . \tag{5.10}$$

For $\phi = 0$ we have the Hadamard matrix:

$$H = \frac{1}{2}\begin{bmatrix} 1 & 1 & 1 & 1 \\ 1 & 1 & -1 & -1 \\ 1 & -1 & 1 & -1 \\ 1 & -1 & -1 & 1 \end{bmatrix} , \tag{5.11}$$

and for $\phi = \pi/2$ we have the Fourier form:

$$F = \frac{1}{2}\begin{bmatrix} 1 & 1 & 1 & 1 \\ 1 & i & -1 & -i \\ 1 & -1 & 1 & -1 \\ 1 & -i & -1 & i \end{bmatrix} . \tag{5.12}$$

5.2 Characterization Method

A multiport beam splitter is represented by a unitary matrix:

$$U = \sum_{kj} u_{kj} e^{i\phi_{kj}} |k\rangle\langle j| , \tag{5.13}$$

for all j, k with $1 < j, k < N$. Where $\{u_{kj}\}$ represent the amplitudes and ϕ_{kj} denotes the relative phases between the cores, which satisfy the conditions $0 <$

$u_{kj} < 1$ and $0 < \phi_{kj} < 2\pi$.

In matrix form, U is expressed as in Eq. (5.1):

$$U = \begin{pmatrix} u_{11}e^{i\phi_{11}} & \cdots & u_{1j}e^{i\phi_{1j}} & \cdots & u_{1N}e^{i\phi_{1N}} \\ \vdots & \ddots & \vdots & & \vdots \\ u_{k1}e^{i\phi_{k1}} & \cdots & u_{kj}e^{i\phi_{kj}} & \cdots & u_{kN}e^{i\phi_{kN}} \\ \vdots & & \vdots & \ddots & \vdots \\ u_{N1}e^{i\phi_{N1}} & \cdots & u_{Nj}e^{i\phi_{Nj}} & \cdots & u_{NN}e^{i\phi_{NN}} \end{pmatrix} . \tag{5.1}$$

The characterization method work as follows [10]:

1. The parameters u_{kj} are the square roots of the split ratios s_{kj}, which can be determined by measuring the probabilities I_{kj} of detecting the photons at the output represented by $|k\rangle$ when the core-mode state $|j\rangle$ was sent through the MBS. It is written as

$$u_{kj} = \sqrt{s_{kj}} = \sqrt{\frac{I_{kj}}{\sum_k I_{kj}}} , \tag{5.14}$$

Where I_{kj} is related with the beam power P_{kj} as follows, $P_{kj} = I_{kj}A_{kj}$. With A_{kj} the mode area, which is consider to be the same in all output ports. In this way,

$$s_{kj} = \frac{P_{kj}}{\sum_k P_{kj}} . \tag{5.15}$$

As shown in Figure 5.1, it is possible to measure P_{kj} in the output port k, by sending light from the input port j of the multiport, while other input modes are in the vacuum state.

Therefore, we can construct the amplitude matrix:

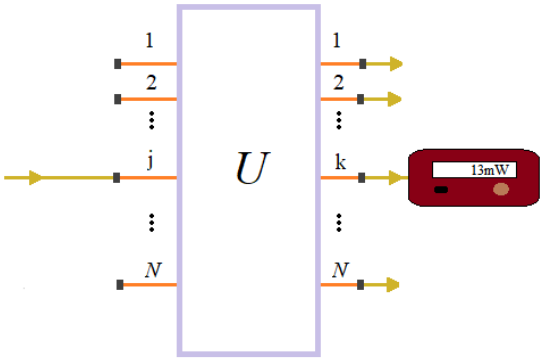

Figure 5.1: Scheme to determine split ratio, part 1 of the protocol. U is the multiport beam splitter with N input ports and N output ports. The power meter is represented by a burgundy rectangle.

$$U_u = \begin{pmatrix} u_{11} & \cdots & u_{1j} & \cdots & u_{1N} \\ \vdots & \ddots & \vdots & & \vdots \\ u_{k1} & \cdots & u_{kj} & \cdots & u_{kN} \\ \vdots & & \vdots & \ddots & \vdots \\ u_{N1} & \cdots & u_{Nj} & \cdots & u_{NN} \end{pmatrix} .$$

2.1 To measure the relative phases, we prepare and send the input state

$$|\psi_j\rangle = \frac{1}{\sqrt{2}}\left(|1\rangle + e^{i\varphi}|j\rangle\right) , \tag{5.16}$$

through the MBS, see Fig. 5.2, where the mode $|1\rangle$ goes to input port 1 and $e^{i\varphi}|j\rangle$ goes to input port j.

The resulting state is given by:

$$U|\psi_j\rangle = \frac{1}{\sqrt{2}}\sum_k \left(u_{k1}e^{i\phi_{k1}} + u_{kj}e^{i(\phi_{kj}+\varphi)}\right)|k\rangle . \tag{5.17}$$

The probability distribution to detect photons in the output mode k of the

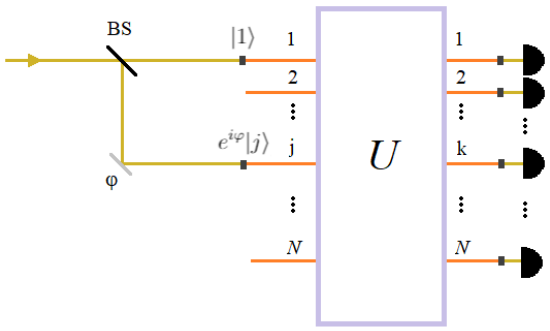

Figure 5.2: Scheme to determine de relative phases. U corresponds to the MBS matrix, BS is a 2×2 beam splitter, φ the phase shifter and half-circles are detectors.

MBS for the inputs j and 1, while φ of the input state is varied, is:

$$\begin{aligned} p(k|j) &= \frac{1}{2}|u_{k1}e^{i\phi_{k1}} + u_{kj}e^{i(\varphi+\phi_{kj})}|^2 \\ &= \frac{1}{2}\left[u_{k1}^2 + u_{kj}^2 + 2u_{k1}u_{kj}\cos(\varphi + \phi_{kj} - \phi_{k1})\right] \ . \end{aligned} \tag{5.18}$$

Hence, by recording the probabilities $p(k|j)$ with respect to j, one can obtain the relative phases $\phi_{kj} - \phi_{k1}$, by fitting this function with a sinusoidal model. However, note that only $N^2 - 2N + 1$ of the phases ϕ_{kj} are physically significant since $2N - 1$ phases can be included into the basis vectors or externally controlled by phase modulators (PM) [10; 17; 51]. Therefore, without loss of generality, we can consider that $\phi_{k1} = \phi_{1j} = 0$, in order to get the real border estimate (see section 2. eq. (5.2)). Then,

$$p(k|j) = \frac{1}{2}\left[u_{k1}^2 + u_{kj}^2 + 2u_{k1}u_{kj}\cos(\varphi + \phi_{kj})\right] \ . \tag{5.19}$$

is the probability of having light in the output mode k for the inputs mode j and 1 of the MBS. In orden to obtain all relative phases ϕ_{kj}, we take first $j = 2$ and measure the outcomes, and then repeat this procedure for all $j = 3, ..., N$. The phase matrix after applying the conditions will be:

$$U_\phi = \begin{pmatrix} 0 & & \cdots & & & 0 \\ & \phi_{22} & \cdots & \phi_{2j} & \cdots & \phi_{2N} \\ \vdots & \vdots & \ddots & \vdots & & \vdots \\ & \phi_{k2} & \cdots & \phi_{kj} & \cdots & \phi_{kN} \\ & \vdots & & \vdots & \ddots & \vdots \\ 0 & \phi_{N2} & \cdots & \phi_{Nj} & \cdots & \phi_{NN} \end{pmatrix} .$$

2.2. We define the fitting function as follows:

$$\bar{p}(k|j) \sim \cos(\varphi + \bar{\phi}_{kj}) \ . \tag{5.20}$$

In the experiment, it is always possible to measure $\bar{\phi}_{1j} \neq 0$. Then, to apply the condition above, we subtract the value $\bar{\phi}_{1j}$ from all the phases $\bar{\phi}_{kj}$ obtained when an initial state was sent to the MBS (that is when j has a fix value), and then redefine the variables. That is,

$$\tilde{\phi}_{1j} = \bar{\phi}_{1j} - \bar{\phi}_{1j}, \tag{5.21}$$

$$\tilde{\phi}_{2j} = \bar{\phi}_{2j} - \bar{\phi}_{1j}, \tag{5.22}$$

$$\vdots \tag{5.23}$$

$$\tilde{\phi}_{Nj} = \bar{\phi}_{Nj} - \bar{\phi}_{1j} \ , \tag{5.24}$$

then, the phase matrix will be:

$$\begin{pmatrix} 0 & \bar{\phi}_{12} & \cdots & \bar{\phi}_{1j} & \cdots & \bar{\phi}_{1N} \\ & \bar{\phi}_{22} & \cdots & \bar{\phi}_{2j} & \cdots & \bar{\phi}_{2N} \\ \vdots & \vdots & \ddots & \vdots & & \vdots \\ & \bar{\phi}_{k2} & \cdots & \bar{\phi}_{kj} & \cdots & \bar{\phi}_{kN} \\ & \vdots & & \vdots & \ddots & \vdots \\ 0 & \bar{\phi}_{N2} & \cdots & \bar{\phi}_{Nj} & \cdots & \bar{\phi}_{NN} \end{pmatrix} \longrightarrow \begin{pmatrix} 0 & & \cdots & & & 0 \\ & \tilde{\phi}_{22} & \cdots & \tilde{\phi}_{2j} & \cdots & \tilde{\phi}_{2N} \\ \vdots & \vdots & \ddots & \vdots & & \vdots \\ & \tilde{\phi}_{k2} & \cdots & \tilde{\phi}_{kj} & \cdots & \tilde{\phi}_{kN} \\ & \vdots & & \vdots & \ddots & \vdots \\ 0 & \tilde{\phi}_{N2} & \cdots & \tilde{\phi}_{Nj} & \cdots & \tilde{\phi}_{NN} \end{pmatrix} .$$

Let $\{\tilde{u}_{jk}\}$ and $\{\tilde{\phi}_{jk}\}$ be the experimental amplitudes and phases, respectively. Then, construct the experimental estimate:

$$\tilde{U} = \sum_{jk} \tilde{u}_{kj} e^{i\tilde{\phi}_{kj}} |k\rangle\langle j| \ , \tag{5.25}$$

which in matrix form is expressed as:

$$\tilde{U} = \begin{pmatrix} \tilde{u}_{11} & \cdots & & \tilde{u}_{1j} & \cdots & \tilde{u}_{1N} \\ & \tilde{u}_{22}e^{i\tilde{\phi}_{22}} & \cdots & \tilde{u}_{2j}e^{i\tilde{\phi}_{2j}} & \cdots & \tilde{u}_{2N}e^{i\tilde{\phi}_{2N}} \\ \vdots & \vdots & \ddots & \vdots & & \vdots \\ \tilde{u}_{k1} & \tilde{u}_{k2}e^{i\tilde{\phi}_{k2}} & \cdots & \tilde{u}_{kj}e^{i\tilde{\phi}_{kj}} & \cdots & \tilde{u}_{kN}e^{i\tilde{\phi}_{kN}} \\ & \vdots & & \vdots & \ddots & \vdots \\ \tilde{u}_{N1} & \tilde{u}_{N2}e^{i\tilde{\phi}_{N2}} & \cdots & \tilde{u}_{Nj}e^{i\tilde{\phi}_{Nj}} & \cdots & \tilde{u}_{NN}e^{i\tilde{\phi}_{NN}} \end{pmatrix} .$$

Due to inherent experimental errors, this estimate is not a unitary matrix. Thereby, the next step is to search for the nearest unitary matrix to $\tilde{U}$ by implementing an optimization method.

5.3 Optimization Method

Let $\hat{U}$ be the nearest unitary matrix to the experimental one, $\tilde{U}$, for the multiport beam splitter. In order to obtain $\hat{U}$ we optimize a cost function of the experimental data. A figure of merit is the Fidelity between two unitary matrices [52] [53]:

$$F(A,B) = \frac{1}{d}|Tr(A^{\dagger}B)|^2 \ . \tag{5.26}$$

This is equivalent to the fidelity between the quantum states associated to A and B by the Choi-Jamiolkowski map. This Fidelity can be easily extended to the case of unitary processes with noise as,

$$F(A,B) = \frac{|Tr(A^{\dagger}B)|^2}{\sqrt{Tr(A^{\dagger}A)Tr(B^{\dagger}B)}} \ , \tag{5.27}$$

a expression that is very useful in our case, since the experimental matrix is not unitary. We employed equation (5.27) to minimize the infidelity between the experimental matrix $\tilde{U}$ and a real border unitary matrix V. Then, the optimized matrix is given by the following minimization:

$$\hat{U} = \arg\min \ \ [1 - F(\tilde{U}, V)] \ , \tag{5.28}$$

that can be solved numerically.

Chapter 6

Experimental Arrangement

Summary

In this chapter, we explain the experimental procedure used to characterize the Multiport Beam Splitter, based on the method detailed in the previous chapter. We described the two main measurement schemes for the determination of the relative phases and the split ratio, and the measurement procedures realized.

6.1 Measurements to determine relative phases

The setup used to determine the relative phases of the matrix is ilustrated in Fig. 6.1. According to the theoretical method, we first had to prepare and send the initial state $|\psi_2\rangle = \frac{1}{\sqrt{2}}(|1\rangle + e^{i\varphi}|2\rangle)$ to the Multiport Beam Splitter (MBS). To accomplish this, a 1546 nm beam is generated by a continuous wave laser source and sent to a Mach Zehnder interferometer device (MZ), which generates few photon pulses, which in turn are sent through a fiber standard 2×2 beam splitter (BS). The relative phase φ was controlled with an electronic phase modulator (PM) in the path $e^{\varphi}|j\rangle$. The path-modes $|1\rangle$ and $e^{\varphi}|j\rangle$ of the BS are conected to

paths $|1\rangle$ and $|j\rangle$, respectively, of the MBS, by means of a demultiplexer (demux1), which allow us to access every core of the MBS. Once the beams passed through the MBS, and the unit transformation is applied over the initial state, we measured the number of photons in each output port of the MBS. Simple count events were recorded with avalanche photodiode detectors (APD's), numbered as shown in Fig. 6.1, while the phase modulator varied the phase φ, in a controlled way, for at least three minutes. In order to measure in the MBS output ports we used a second demultiplexer (demux2). Detector numbering labels correspond to the numbering of the MBS output ports. Pulses in the MZ and detecttion gates synchronization are controled by a field-programmable gate array (FPGA).

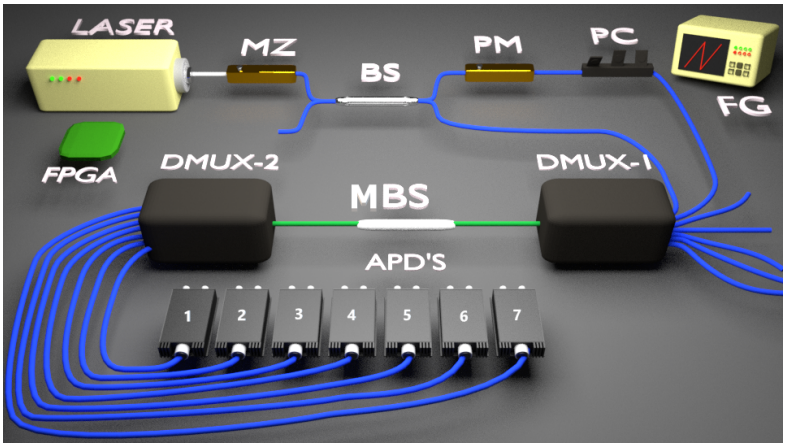

Figure 6.1: Experimental Setup. MZ: electronic mach zehnder interferometer; BS: 2×2 beam splitter; PM: phase modulator, PC: polarization controler; FG: funtion generation, demux1(2): MCF spatial demultiplexers; MBS: Multiport Beam Splitter; APD's: Avalanche Photodiode detectors; FPGA: field-programmable gate array. Detector numbering labels correspond to the numbering of the MBS output ports.

By repeating this procedure with another input state, such as $|\psi_3\rangle$, and then with others until $j = N$, we could be able to collect all the relative phases ϕ. The data recorded by each detector were utilized to plot variations of simple counts $I(s.c.)$ as a function of the modulated phase $\varphi(t)$, resulting in N curves (graphs)

when a configuration of an initial state was sent.

6.1.1 Case of 4×4 MBS

We first prepared and sent the initial state $|\psi_2\rangle = \frac{1}{\sqrt{2}}(|1\rangle + e^{i\varphi}|2\rangle)$ to the 4×4 MBS, and, at the same time, we measured the number of photons detected with the APD's in the output ports 1, 2, 3 and 4 of this MBS, while the phase modulator varied the phase φ, in a controlled way. Then, we repeat this process by sending the other input states ($|\psi_3\rangle$ and $|\psi_4\rangle$), obtaining four curves per input state sent. We note that for each input state that was sent to the 4×4 MBS, the period of the resulting four curves was the same. However, this period was not constant in each of the curves due to phase noise of the fibers caused by mechanical and thermal variations on them. One way to solve this problem was to select a data set with a constant period T from graph-1, whose data range goes from φ_0 to φ_1 (or equivalently in time from t_0 to t_1). And we used this same interval of time to select the data from the other curves. In this way, four curves with exactly the same period T were obtained for an input state sent.

6.1.2 Case of 7×7 MBS

A diagram of the geometry of the 7×7 MBS is shown in Fig. 6.2.

To follow the protocol, we need to use seven APD's detectors, however, we had avaliable only four. Then, we first prepared and sent the initial state $|\psi_2\rangle$ to the 7×7 MBS, and at the same time, we measured the number of photons detected in the output ports 1, 2, 3 and 4 of this multiport. Subsequently, to measure the remaining output ports 5, 6 and 7, for this input state, we used the same set of detectors. We left the connection of detector 1 fixed to output port 1 of the 7×7 MBS, and the other detectors were connected the outputs 5, 6 and 7 of the multiport, and continued with the measurement. Then, we repeat this process by

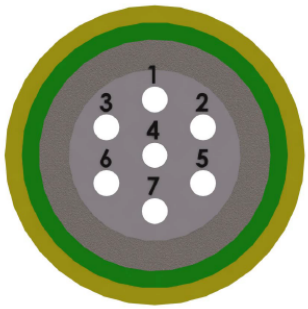

Figure 6.2: Diagram showing geometry (Cross-section) and labelling of paths in the 7×7 MBS.

sending the other input states ($|\psi_3\rangle$, $|\psi_4\rangle$, $|\psi_5\rangle$, $|\psi_6\rangle$ and $|\psi_7\rangle$). We obtained a total of eight curves: graph-1, graph-2, graph-3, graph-4, graph-1', graph-5, graph-6 and graph-7, per input state sent. Therefore, we seleted a range of the data of graph-1 and graph-1', with the same constant period T, and utilized this same interval to select the data in other curves. Finally, we repeat this data processing with the other configuration of input states sent.

6.2 Measurements to determine the split ratio

According to the characterization method, to obtain all the amplitudes of the characteristic matrix we need to determine the transmission probabilities (split ratio) of each core of the MBS. To do that, we use the element set demux1 - MBS - demux2 of the Fig.6.1 in order to access all MBS cores. The scheme of measurement is shown in Fig.6.3, for the case of 7×7 MBS, but it is the same idea for the case of 4×4 MBS.

The determination of the split ratio consisted in sending a 1550 nm beam of 17.69 mW from path 1 of the demux1 and measure the maximum power in path 1 of the demux2, from left to right. Then, we measured the power in other paths of the demux2, keeping the same path of the demux1 illuminated. Finally, we repeated

this procedure by sending light from the other demux 1 paths, separately, until we complete them all.

All the fibers are connected to each other through connectors, C_1 and C_2, which introduce an attenuation of the propagating beam, it is called connection loss. To minimize this loss, it was necessary to maximize the intensity between two connected fibers and to achieve this, the connector that connects them should be moved until reaching the maximum power of the beam. Keeping that in mind, we followed the next procedure to maximize the first path of the system.

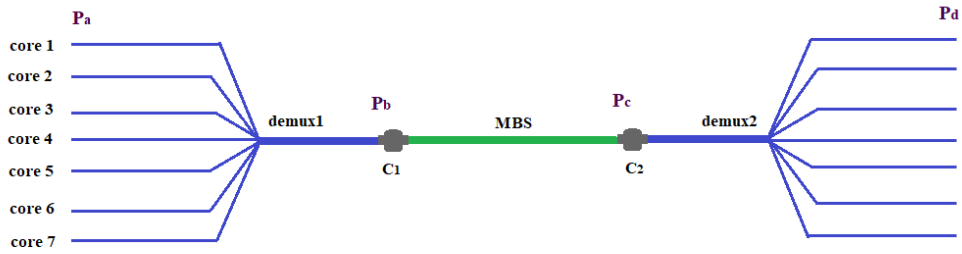

Figure 6.3: Scheme to determine the split ratio of a MBS. The case of the 7×7 MBS is shown in this figure. demux1(2): MCF spatial demultiplexers; MBS: Multiport Beam Splitter; $C_{1,2}$: connectors; P_j: system input power, P_{jk}: system output power.

First, we sent the beam from the path 1 of the demux1 (from left to right), and by moving the connector C_1, we maximized the light power at the end of the MBS using a power meter. Afterward, we connected the free end of the MBS to the demux2, using a second connector, C_2, and maximize the intensity at the end of the path 1 of the demux2, by moving the conector C_2. Then, we continued with the procedure described above.

All 7×7 MBS measured powers are shown in the Table 6.1 following the notation P_{jk}. It represents the power measured in the core k of the demux2, when a beam is sent from the core j of the demux1. The power $\sum_k P_{jk}$ that results from adding all the powers of the cores k for the same j is also shown. Power error

was assumed to be the instrumental error of the Power Meter. Other errors were calculated using error propagation.

$P_{jk} \pm 0.01$ mW	P_{1k}	P_{2k}	P_{3k}	P_{4k}	P_{5k}	P_{6k}	P_{7k}
P_{j1}	1.52	0.31	0.74	1.51	2.00	0.09	1.50
P_{j2}	0.23	0.29	3.64	1.61	1.60	1.61	0.37
P_{j3}	0.62	3.61	0.20	1.22	0.13	0.65	1.40
P_{j4}	0.74	0.84	0.83	1.29	0.99	1.22	2.31
P_{j5}	0.66	1.05	0.28	0.85	0.05	5.22	1.26
P_{j6}	0.11	1.21	1.00	1.87	2.93	0.60	0.17
P_{j7}	0.82	0.25	1.41	2.14	0.76	0.18	2.07
$\sum_k P_{jk} \pm 0.03$ mW	4.69	7.56	8.10	10.51	8.45	9.56	9.08

Table 6.1: Data measured for the split ratio determination of the 7×7 MBS. P_{jk}: power measured in the output core k of the demux2, when a beam of 17.69 mW is sent from the input core j of the demux1 (See Fig. 6.3).

6.3 Measurement to determine connection loss

6.3.1 Case 4×4 MBS

To determine the loss both connectors, t_{C1} and t_{c2}, the arrangement of the Fig. 6.4 was used. We sent a beam of 1550 nm trough the demux-i's core 1, and measured the power $P_b^{(i)}$ before the connector C_i with the power meter (with $i = 1, 2$, depending on the connector loss we want to determine). Then, we connected the demux-i with the multicore fiber using the connector C_i, and finally, measured the power $P_c^{(i)}$ at the end of this MCF. This procedure was performed for each path, obtaining four values of $P_b^{(i)}$ and four values of $P_c^{(i)}$.

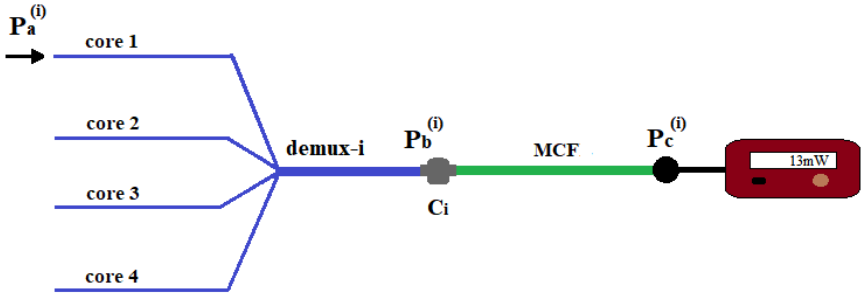

Figure 6.4: Scheme to determine the connection loss of a MBS. C_i: conector i (depending on the connection loss we want to determine, we used $i = 1$ or $i = 2$); MCF: Multicore Fiber; P_a: input power, P_b: power before C_i; P_c: power after MCF.

With the powers measured above, we determine an average for the loss of connector 1:

$$\langle t_{C1} \rangle = \left\langle \frac{P_c^{(1)}}{P_b^{(1)}} \right\rangle = 0.944 \pm 0.002 \ . \tag{6.1}$$

Similarly, the loss of connector 2 is estimated

$$\langle t_{C2} \rangle = \left\langle \frac{P_c^{(2)}}{P_b^{(2)}} \right\rangle = 0.9584 \pm 0.0001 \ . \tag{6.2}$$

6.3.2 Case 7×7 MBS

Similar to the case 4×4 MBS we measured the connection loss of 7×7 system. The result was, $\langle t_{C1} \rangle = 0.78 \pm 0.027$ and $\langle t_{C2} \rangle = 0.81 \pm 0.08$. However, we consider this result as not satisfactory, due to the great loss of light that implies in the system and because of the the high error reported. A difference in the dimensions of the MCF and the demux could have caused this result. For example, the MCF's cores were more separated than the demux's cores, the fibers' diameters were not the same, etc.

According to the paper Connector Type Fan-out Device for Multi-core Fiber of Osamu SHIMAKAWA, et al. [54], it could be estimated that the connection

transmission should be in average $\langle t_{C1} \rangle = \langle t_{C2} \rangle = 0.94 \pm 0.04$ (we will assume that both connectors are equal), given a certain angle of disalignment less than one degree. We consider this value later to determine the transmission average of the 7×7 MBS.

Chapter 7

Results and Analysis

Summary

In this seccion we show the values measured in the previous chapter, which were used to determine the relative phases and the amplitudes of the matrices of 4×4 MBS and 7×7 MBS. Following the protocol, we finally obtained an optimized unitary matrix for this multiports with their respective errors. We also present an analysis, interpretation and evaluation of the results.

7.1 Experimental results

Results will be shown in two cases, depending on the MBS used (if the device was of 4 or 7 cores). In both cases, we used the Origin program to determine the relative phases, fitting the graphs of the experimental measurements with a sinusoidal function $\cos^2(\varphi + \bar{\phi}_{kj})$, where $\varphi = \omega x$. The fitting function gave us experimental phases $\bar{\phi}_{kj}$ and their associated errors for the curves when setting the known frequency ω in the software, while x represents the time. With this procedure N phases were determined (with N the number of output ports of the

MBS) when an initial state was sent. According to the characterization protocol, we need to set $\bar{\phi}_{k1} = \bar{\phi}_{1j} = 0$. Experimentally we can not measure $\bar{\phi}_{k1}$ with our setup and protocol, so we directly set $\bar{\phi}_{k1} = 0$, but it is not the same for $\bar{\phi}_{1j}$. To apply this last condition, we subtract the value $\bar{\phi}_{1j}$ from all the phases $\bar{\phi}_{kj}$ obtained when an initial state was sent to the MBS. The experimental phases determined with this protocol are:

$$\tilde{\phi}_{1j} = \bar{\phi}_{1j} - \bar{\phi}_{1j}, \tag{7.1}$$

$$\tilde{\phi}_{2j} = \bar{\phi}_{2j} - \bar{\phi}_{1j}, \tag{7.2}$$

$$\vdots \tag{7.3}$$

$$\tilde{\phi}_{Nj} = \bar{\phi}_{Nj} - \bar{\phi}_{1j} \tag{7.4}$$

7.1.1 Case 7×7 MBS

The relative phases estimated for the 7×7 MBS are presented in the Table 7.1. We observe that the first column has totally zero values, in total agreement with the equation (5.18) of the protocol, where it is clear the phase had to be zero when the input state $|\psi_1\rangle$ was sent to the MBS.

Now, according to the equation (5.15) of the protocol, we constructed an approximation of the split ratio of the 7×7 MBS by using the powers P_{jk} of the Table 6.1. The results of this approximation is shown in Table 7.2. Values and errors are shown in separate tables for space and clarity only. Here we observe the distribution of the light in the MBS is non-uniform and could follow a second-neighbor interaction.

Next, with the values of the split ratio approximation of the Table 7.2 we could determine the amplitudes table by applying the equation 5.14 of the protocol. These values are shown in the table 7.3.

ϕ_{jk}	ϕ_{1k}	ϕ_{2k}	ϕ_{3k}	ϕ_{4k}	ϕ_{5k}	ϕ_{6k}	ϕ_{7k}
ϕ_{j1}	0.00	0.00	0.00	0.00	0.00	0.00	0.00
ϕ_{j2}	0.00	1.56	3.69	-0.25	1.88	-0.71	4.09
ϕ_{j3}	0.00	3.63	-0.75	4.02	2.09	-1.29	1.47
ϕ_{j4}	0.00	0.09	4.28	2.03	-1.66	3.78	2.26
ϕ_{j5}	0.00	2.15	2.44	-1.80	-1.13	1.90	3.33
ϕ_{j6}	0.00	0.46	-0.33	4.34	2.59	3.63	0.08
ϕ_{j7}	0.00	4.50	1.59	2.17	3.21	-0.73	-1.35
$\pm\Delta\phi_{jk}$	$\pm\Delta\phi_{1k}$	$\pm\Delta\phi_{2k}$	$\pm\Delta\phi_{3k}$	$\pm\Delta\phi_{4k}$	$\pm\Delta\phi_{5k}$	$\pm\Delta\phi_{6k}$	$\pm\Delta\phi_{7k}$
$\pm\Delta\phi_{j1}$	0.00	0.04	0.07	0.05	0.05	0.05	0.05
$\pm\Delta\phi_{j2}$	0.00	0.04	0.06	0.05	0.06	0.04	0.08
$\pm\Delta\phi_{j3}$	0.00	0.04	0.08	0.04	0.06	0.04	0.06
$\pm\Delta\phi_{j4}$	0.00	0.04	0.06	0.05	0.04	0.04	0.05
$\pm\Delta\phi_{j5}$	0.00	0.04	0.06	0.06	0.05	0.04	0.04
$\pm\Delta\phi_{j6}$	0.00	0.07	0.06	0.05	0.06	0.07	0.06
$\pm\Delta\phi_{j7}$	0.00	0.05	0.05	0.04	0.05	0.05	0.04

Table 7.1: Estimation of the relative phases $\phi_{jk} \pm \Delta\phi_{jk}$ of the 7×7 MBS matrix.

s_{jk}	s_{1k}	s_{2k}	s_{3k}	s_{4k}	s_{5k}	s_{6k}	s_{7k}
s_{j1}	0.324	0.042	0.092	0.144	0.237	0.009	0.165
s_{j2}	0.049	0.039	0.449	0.153	0.189	0.168	0.040
s_{j3}	0.132	0.478	0.024	0.117	0.015	0.068	0.154
s_{j4}	0.157	0.111	0.102	0.123	0.117	0.128	0.254
s_{j5}	0.140	0.139	0.035	0.081	0.005	0.546	0.139
s_{j6}	0.024	0.159	0.123	0.178	0.347	0.062	0.019
s_{j7}	0.174	0.033	0.174	0.204	0.089	0.018	0.229
$\pm\Delta s_{jk}$	$\pm\Delta s_{1k}$	$\pm\Delta s_{2k}$	$\pm\Delta s_{3k}$	$\pm\Delta s_{4k}$	$\pm\Delta s_{5k}$	$\pm\Delta s_{6k}$	$\pm\Delta s_{7k}$
$\pm\Delta s_{j1}$	0.003	0.001	0.001	0.001	0.001	0.001	0.001
$\pm\Delta s_{j2}$	0.002	0.001	0.002	0.001	0.001	0.001	0.001
$\pm\Delta s_{j3}$	0.002	0.002	0.001	0.001	0.001	0.001	0.001
$\pm\Delta s_{j4}$	0.002	0.001	0.001	0.001	0.001	0.001	0.001
$\pm\Delta s_{j5}$	0.002	0.001	0.001	0.001	0.001	0.002	0.001
$\pm\Delta s_{j6}$	0.002	0.001	0.001	0.001	0.002	0.001	0.001
$\pm\Delta s_{j7}$	0.002	0.001	0.001	0.001	0.001	0.001	0.001

Table 7.2: MBS split ratio approximation, where $s_{jk} = P_{jk} / \sum_k P_{jk}$ and $\pm\Delta s_{jk}$ refers to experimental error.

u_{jk}	u_{1k}	u_{2k}	u_{3k}	u_{4k}	u_{5k}	u_{6k}	u_{7k}
u_{j1}	0.569	0.204	0.303	0.380	0.487	0.095	0.406
u_{j2}	0.221	0.196	0.670	0.392	0.434	0.410	0.201
u_{j3}	0.363	0.691	0.156	0.341	0.124	0.260	0.393
u_{j4}	0.396	0.332	0.320	0.350	0.343	0.357	0.504
u_{j5}	0.375	0.373	0.186	0.285	0.073	0.739	0.372
u_{j6}	0.154	0.399	0.351	0.422	0.589	0.250	0.138
u_{j7}	0.417	0.181	0.418	0.452	0.299	0.136	0.478
$\pm\Delta u_{jk}$	$\pm\Delta u_{1k}$	$\pm\Delta u_{2k}$	$\pm\Delta u_{3k}$	$\pm\Delta u_{4k}$	$\pm\Delta u_{5k}$	$\pm\Delta u_{6k}$	$\pm\Delta u_{7k}$
$\pm\Delta u_{j1}$	0.002	0.003	0.002	0.001	0.001	0.005	0.001
$\pm\Delta u_{j2}$	0.005	0.003	0.001	0.001	0.002	0.001	0.003
$\pm\Delta u_{j3}$	0.003	0.002	0.004	0.001	0.005	0.002	0.002
$\pm\Delta u_{j4}$	0.003	0.002	0.002	0.001	0.002	0.002	0.001
$\pm\Delta u_{j5}$	0.003	0.002	0.003	0.002	0.008	0.001	0.002
$\pm\Delta u_{j6}$	0.007	0.002	0.002	0.001	0.001	0.002	0.004
$\pm\Delta u_{j7}$	0.003	0.004	0.002	0.001	0.002	0.004	0.001

Table 7.3: Amplitudes $u_{jk} \pm \Delta u_{jk}$.

Replacing the values of u_{jk} and θ_{jk} of the tables 7.3 and 7.1, respectively, in the equation (5.25), we determined the components of the matrix $\tilde{U}_{7\times7}$ shown in (7.5). Errors are not presented in the matrix.

$$\tilde{U}_7 = \begin{bmatrix} 0.569 & 0.204 & 0.302 & 0.380 & 0.487 & 0.095 & 0.406 \\ 0.221 & 0.196i & -0.566-0.359i & 0.379-0.097i & -0.121+0.417i & 0.316-0.261i & -0.118-0.163i \\ 0.364 & -0.616-0.314i & 0.114-0.107i & -0.218-0.263i & 0.060+0.109i & 0.073-0.250i & 0.037+0.391i \\ 0.396 & 0.331+0.031i & -0.136-0.290i & -0.159+0.312i & -0.032-0.341i & -0.283-0.219i & -0.321+0.388i \\ 0.375 & -0.200+0.315i & -0.144+0.119i & -0.062-0.278i & 0.031-0.066i & -0.250+0.696i & -0.366-0.070i \\ 0.154 & 0.356+0.181i & 0.330-0.119i & -0.156-0.3393i & -0.497+0.316i & -0.219-0.120i & 0.137+0.009i \\ 0.417 & -0.040-0.177i & -0.013+0.417i & -0.254+0.373i & -0.298-0.019i & 0.102-0.090i & 0.104-0.467i \end{bmatrix} \tag{7.5}$$

In the Fig. 7.1 it is shown the test of unitarity $\tilde{U}_7^\dagger \tilde{U}_7$ of the experimental matrix. There, we can see that due to experimental errors the estimated matrix is not exactly a unitary matrix, but a near-unitary one. However, for experimental data they are quite good. The next step is to apply the optimization method described in the section section 5.3 of chap. 5.

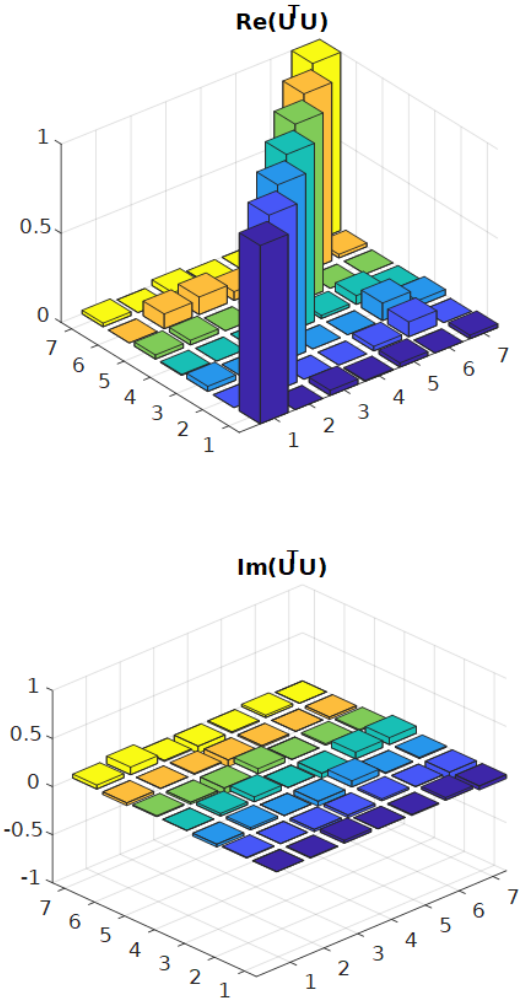

Figure 7.1: Unitarity Test of $\tilde{U}_7$. Real and imaginary part at left and right, respectively

In this way, the corresponding unitary matrix $\hat{U}$ that results from implementing

the optimization method is:

$$\hat{U}_7 = \begin{bmatrix} 0.564 & 0.201 & 0.302 & 0.375 & 0.492 & 0.091 & 0.400 \\ 0.222 & -0.007+0.187i & -0.570-0.306i & 0.356-0.087i & -0.145+0.363i & 0.299-0.288i & -0.103-0.164i \\ 0.349 & -0.627-0.310i & 0.118-0.099i & -0.225-0.269i & 0.047+0.108i & 0.063-0.245i & 0.012+0.406i \\ 0.393 & 0.332+0.016i & -0.162-0.295i & -0.127+0.335i & -0.049-0.341i & -0.332-0.145i & -0.345+0.353i \\ 0.371 & -0.184+0.289i & -0.120+0.107i & -0.022-0.270i & 0.021-0.053i & -0.014+0.722i & -0.342-0.070i \\ 0.147 & 0.371+0.203i & 0.357-0.096i & -0.094-0.432i & -0.526+0.304i & -0.279-0.055i & 0.135+0.011i \\ 0.444 & -0.022-0.170i & -0.065+0.433i & -0.316+0.325i & -0.316-0.020i & 0.084-0.121i & 0.099-0.494i \end{bmatrix} \tag{7.6}$$

Note that this matrix is not symmetric, that is, its coefficients have absolute value different than $1\sqrt{7}$. Though we do not yet have a complete theoretical model, this is what one intuitively expects based on simple considerations concerning the geometry of the cores in the fiber. For this reason this approximation matrix will not be compared with a theoretical model, but wih the experimental one. The fidelity between the experimental matrix and the unitary one is

$$F(\tilde{U}_7, \hat{U}_7) = 0.992 \pm 0.008 \ . \tag{7.7}$$

Which is a satisfactory result, as expected. We note that recent results [55] have shown that even non-symmetric N-port beam splitter devices can serve as primitives for construction of a universal device that implements any $N \times N$ unitary.

7.1.2 Case 4×4 MBS

The relative phases estimated for the multiport Beam Splitter of 4 cores (4×4 MBS), which is illustrated in Fig. 4.1.b) of the chapter 4, are presented in the Table 7.4. We observed that the first column has values equal to zero, in total agreement with the equation (5.18), where it is clear the phase had to be zero when the input state $|\psi_1\rangle$ was sent to the multiport.

For the case of 4×4 MBS we use the intensity values previously measured

ϕ_{jk}	ϕ_{1k}	ϕ_{2k}	ϕ_{3k}	ϕ_{4k}
ϕ_{j1}	0.00	0.00	0.00	0.00
ϕ_{j2}	0.00	-3.02	0.05	-3.21
ϕ_{j3}	0.00	0.15	3.22	-3.10
ϕ_{j4}	0.00	-3.13	3.01	-0.06
$\pm\Delta\phi_{jk}$	$\pm\Delta\phi_{1k}$	$\pm\Delta\phi_{2k}$	$\pm\Delta\phi_{3k}$	$\pm\Delta\phi_{4k}$
$\pm\Delta\phi_{j1}$	0.00	0.05	0.08	0.04
$\pm\Delta\phi_{j2}$	0.00	0.05	0.09	0.05
$\pm\Delta\phi_{j3}$	0.00	0.04	0.08	0.05
$\pm\Delta\phi_{j4}$	0.00	0.06	0.08	0.04

Table 7.4: Estimation of the relative phases $\phi_{jk} \pm \Delta\phi_{jk}$ of the 4×4 MBS matrix.

using an imaging system consisted of a 10× objective lens to generate the enlarged image of the MBS output, with a 100 μm mobile pinhole placed at the image point, attached to a power meter. A 1550 nm beam was sent to an input core of the MBS and the power of each of the images of the cores were registered. This procedure were repeated with all the input core of the MBS. The power at each output core is stable and the observed average split ratio was 0.25 ± 0.01 as shown in Fig. 7.2.b). With these values it is possible to construct the Table 7.5 for the amplitudes.

u_{jk}	u_{1k}	u_{2k}	u_{3k}	u_{4k}
u_{j1}	0.50	0.50	0.50	0.50
u_{j2}	0.50	0.50	0.50	0.50
u_{j3}	0.50	0.50	0.50	0.50
u_{j4}	0.50	0.50	0.50	0.50
$\pm\Delta u_{jk}$	$\pm\Delta u_{1k}$	$\pm\Delta u_{2k}$	$\pm\Delta u_{3k}$	$\pm\Delta u_{4k}$
$\pm\Delta u_{j1}$	0.01	0.01	0.01	0.01
$\pm\Delta u_{j2}$	0.01	0.01	0.01	0.01
$\pm\Delta u_{j3}$	0.01	0.01	0.01	0.01
$\pm\Delta u_{j4}$	0.01	0.01	0.01	0.01

Table 7.5: Estimation of the amplitudes $u_{jk} \pm \Delta u_{jk}$ of the 4×4 MBS matrix.

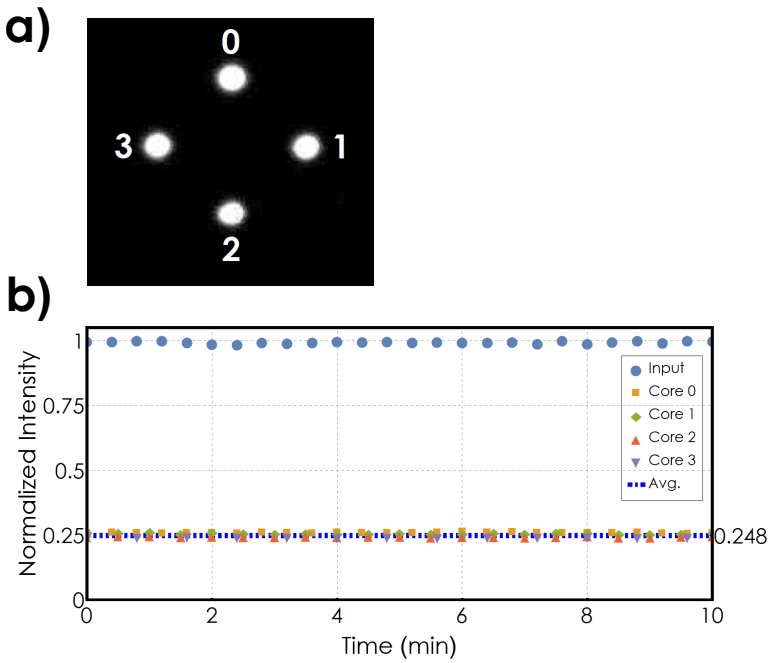

Figure 7.2: 4×4 Multiport beam splitter performance. a) Image of the facet as seen by an infrared CCD camera. b) Output normalized optical power of each core as a function of time.

By applying the protocol we obtained the following experimental estimate:

$$\tilde{U}_4 = \begin{bmatrix} 0.5 & 0.5 & 0.5 & 0.5 \\ 0.5 & 0.493 + 0.07i & 0.497 - 0.05i & -0.499 - 0.01i \\ 0.5 & -0.496 - 0.06i & 0.499 + 0.03i & -0.499 + 0.03i \\ 0.5 & -0.5 & -0.496 + 0.06i & 0.499 - 0.03i \end{bmatrix},$$

In the Fig. 7.3 it is shown the test of unitarity $\tilde{U}_4^{\dagger}\tilde{U}_4$ of the experimental matrix. There, we can see that the estimated matrix is almost a perfect unit matrix. However, we will apply the optimization method described in the protocol to correct the experimental errors.

The corresponding unitary one is:

$$\hat{U}_4 = \begin{bmatrix} 0.499 & 0.501 & 0.499 & 0.499 \\ 0.501 & 0.491 + 0.08i & -0.496 - 0.06i & -0.498 - 0.01i \\ 0.499 & -0.495 - 0.06i & 0.498 + 0.03i & -0.499 + 0.03i \\ 0.499 & -0.499 - 0.01i & -0.499 + 0.03i & 0.499 - 0.01i \end{bmatrix},$$

We have that the fidelity between the experimental estimate and the unitary estimate is

$$F(\tilde{U}_4, \hat{U}_4) = 0.999 \pm 0.001. \tag{7.8}$$

Note that the unitary estimate is almost a symmetric unitary matrix, or equivalently, the absolute value of each coefficient of the matrix is approximately 1/2. Comparing the unitary estimate with the symmetric unitary matrix with $\phi = 0$, eq. (5.11), we have the fidelity

$$F(\tilde{U}_4, H) = 0.995 \pm 0.003. \tag{7.9}$$

Which allows us to confirm that this method is reliable to characterize a multiport.

7.2 Matrix error analisys

We perform Monte Carlo simulations to quantify the error of the estimated matrices. We employ the Gaussian distribution $N(\mu, \sigma)$ for this task, where μ is the mean and σ is the standard deviation. Considering the error as 3 times the standard deviation of the Gaussian distribution, approximately 99.7% of the realizations are inside of the interval $\mu \pm 3\sigma$. Experimentally, we measured the intensities $I_{jk} \pm \Delta I_{jk}$ and the phases $\phi_{jk} \pm \Delta\phi_{jk}$, with ΔI_{jk} and $\Delta\phi_{jk}$ being their

respective experimental errors. Thereby, the simulated split ratios and phases are given by

$$u_{jk} \sim N(u_{jk}, \Delta u_{jk}/3), \qquad \phi_{jk} \sim N(\phi_{jk}, \Delta\phi_{jk}/3) \tag{7.10}$$

respectively. We generate a sample of 10^5 MBS matrices $\tilde{U}$ and $\hat{U}$ independently, and with them we calculate the average fidelity and their respectively errors, which were consider as 3 times the standard deviations.

7.3 Determination of MBS's loss

7.3.1 Case 4×4 MBS

In the Fig. 7.4. we show the scheme of measurement to determine the 4×4 MBS's loss. First, we sent a 1550 nm beam from left to right through the system, and measured the powers P_a and P_b for each demux-1's input. With those values, we determined the average transmission of the 4×4 MBS, t_{BS4}, and the connector-1 together.

$$\langle t_{C1} t_{BS4} \rangle = \left\langle \frac{P_b}{P_a} \right\rangle = 0.822 \pm 0.004 \ . \tag{7.11}$$

Afterward, we repeat this procedure but in the reverse direction, that is, sending light from right to left through the system, and measured the powers P'_a and P'_b for each demux-2's input. With those values, we determined the average transmission of the 4×4 MBS, t_{BS4}, and the connector-2 together, obtaining the following average:

$$\langle t_{C2} t'_{BS4} \rangle = \left\langle \frac{P'_b}{P'_a} \right\rangle = 0.918 \pm 0.001 \ . \tag{7.12}$$

Replacing the calculated values in the ecuations (6.1) and (6.2) into the equations (7.11) and (7.12), respectively, we estimated two average values of the 4×4 MBS transmision:

$$\langle t_{BS4} \rangle = \frac{\langle t_{C1} t_{BS4} \rangle}{\langle t_{C1} \rangle} = 0.87 \pm 0.01 \ . \tag{7.13}$$

$$\langle t'_{BS4} \rangle = \frac{\langle t_{C2} t'_{BS4} \rangle}{\langle t_{C2} \rangle} = 0.957 \pm 0.001 \ . \tag{7.14}$$

Finally, we averaged the values (7.13) and (7.14) and obtained the average value for the 4×4 MBS:

$$T_{BS4} = 0.91 \pm 0.06 \ . \tag{7.15}$$

7.3.2 Case 7×7 MBS

Similarly to the case of 4x4-system we determine the 7×7 MBS's loss, that is using the same scheme shown in 7.4, but with the demux and MBS of 7 ports instead. First, we sent a 1550 nm beam from left to right through the system, and measured the powers P_a and P_b for each demux-1's input. With those values, we determined the average transmission of the 7×7 MBS, t_{BS7}, and the connector-1 together.

$$\langle t_{C1} t_{BS7} \rangle = \left\langle \frac{P_b}{P_a} \right\rangle = 0.82 \pm 0.12 \ . \tag{7.16}$$

Afterward, we repeat this procedure but in the reverse direction, that is, sending light from right to left through the system, and measured the powers P'_a and P'_b for each demux-2's input. With those values, we determined the average transmission of the 7×7 MBS, t_{BS7}, and the connector-2 together, obtaining the following

average:

$$\left\langle t_{C2}t'_{BS7}\right\rangle = \left\langle \frac{P'_b}{P'_a} \right\rangle = 0.86 \pm 0.03 \ . \tag{7.17}$$

We supposed that $\langle t_{C1}\rangle = \langle t_{C2}\rangle = 0.94 \pm 0.04$, to estimate two average values of the 7×7 MBS transmision:

$$\left\langle t_{BS7}\right\rangle = \frac{\left\langle t_{C1}t_{BS7}\right\rangle}{\left\langle t_{C1}\right\rangle} = 0.86 \pm 0.13 \ . \tag{7.18}$$

$$\left\langle t'_{BS7}\right\rangle = \frac{\left\langle t_{C2}t'_{BS7}\right\rangle}{\left\langle t_{C2}\right\rangle} = 0.91 \pm 0.04 \ . \tag{7.19}$$

Finally, we averaged the values (7.18) and (7.19) and obtained the average value for the 7×7 MBS:

$$T_{BS7} = 0.88 \pm 0.03 \ . \tag{7.20}$$

As expected the value of the average transmission of the 7×7 MBS is lower than the 4×4 MBS. Mainly because its geometry was more complex, due to the number of cores, of this multiport.

7.3.3 Optical Depth

Another important aspect is the optical depth, which is defined as the longest path through the interferometer, enumerated by counting the number of beam splitters traversed by that path. In the case of both Multiport Beam Splitters, proposed in this thesis, there is a much shorter optical depth, since it is only a large beam splitter, in which the "light splitting process" occurs by a tunneling effect. Then, the propagation losses in the MBS's are reduced. On the other hand, if we had

to use the standard model of Reck et al to manufacture the multiport devices, we would need twenty-one 2×2-beam splitters for the case of dimension $d = 7$ and six 2×2-beam splitters for the case of dimension $d = 4$, which would clearly imply a much longer optical depth.

However, the Multiport Beam Splitter is not capable of implementing an arbitrary unit transformation, at least for the dimensions $d = 4$ and $d = 7$, while the Reck configuration can perform any transformation on qudits for a given dimension d, that is, it is a universal configuration.

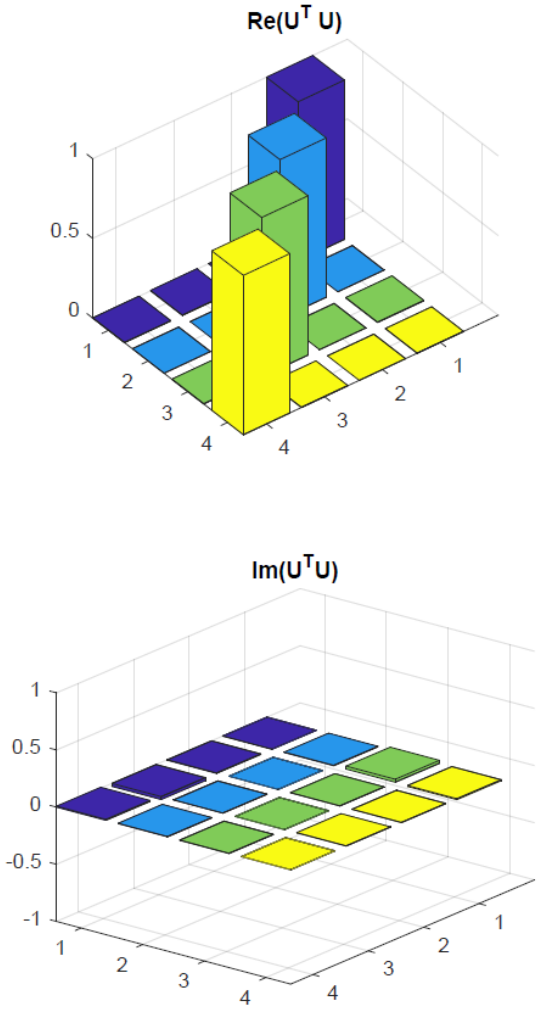

Figure 7.3: Unitarity Test of $\tilde{U}_4$. Real and imaginary part at left and right, respectively

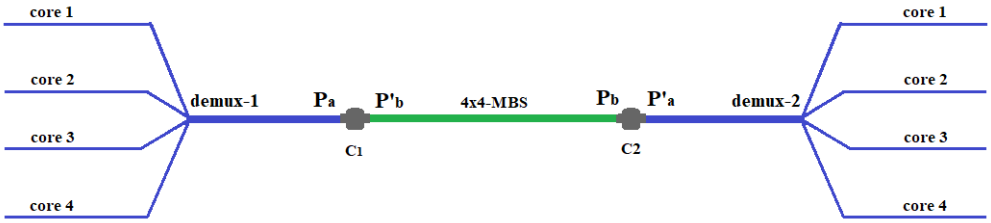

Figure 7.4: Scheme to determine the 4×4 MBS loss. demux-1: demultiplexer-1, demux-2: demultiplexer-2; C_1: connector-1; C_2: connector-2; 4×4 MBS: Multiport Beam Splitter of 4x4 ports; P_a: power before connector-1, and P_b: power before connector-2, when light is sent from left to right. P'_a: power before connector-2, and P'_b: power before connector-1, when light is sent from right to left.

Chapter 8

Applications

Summary

In this section we explore possible applications of the multiport beam splitter by proposing the implementation of a Positive Operator Value Measurements (POVM), focusing on the case of a four-dimensional non-projective measurement with seven outcomes.

8.1 POVM implementation

A POVM is a generalized measurement characterized by semi-defined positive operators E_j, which satisfy the completeness relation $\sum_j E_j = I$, and it can be implemented using an ancilla system. Let $\mathcal{H}_s$ be the state space of the principal system and $\mathcal{H}_a$ the same for the ancilla system, and consider the extended system $\mathcal{H} = \mathcal{H}_s \oplus \mathcal{H}_a$, where $\oplus$ is the direct sum. The dimension of the extended system is $d_s + d_a$, where d_s and d_a are the dimension of $\mathcal{H}_s$ and $\mathcal{H}_a$, respectively.

Let M_j be a projective measurement in $\mathcal{H}$,

$$M_j = |\psi\rangle\langle\psi_j| \ , \qquad j = 0, ..., d-1 \ . \tag{8.1}$$

where

$$|\psi_j\rangle = \sum_{k=0}^{d-1} \langle k|\psi_j\rangle |k\rangle \ \in \mathcal{H} \ , \tag{8.2}$$

It satisfies the completness relation $\sum_j M_j = I$, which can be written as

$$\sum_j \langle k|\psi_j\rangle\langle\psi_j|l\rangle = \delta_{kl}, \qquad j, l = 0, ..., d-1. \tag{8.3}$$

Now, let $|\phi\rangle$ be a state of $\mathcal{H}_s$,

$$|\phi\rangle = \sum_{k=0}^{d_s-1} \langle k|\phi\rangle |k\rangle. \tag{8.4}$$

Clearly, $|\phi\rangle \in \mathcal{H}$. Then, one can measure $|\phi\rangle$ with the set $\{|\psi_j\rangle\}$. The probability to obtain the j-th output is given by

$$\begin{aligned} p_j &= |\langle\psi_j|\phi\rangle|^2 && (8.5)\\ &= \left|\sum_{k=0}^{d_s-1} \langle\psi_j|k\rangle\langle k|\phi\rangle\right|^2 && (8.6)\\ &= \left|\langle\psi_j| \left[\sum_{k=0}^{d_s-1} |k\rangle\langle k|\right] |\phi\rangle\right|^2 && (8.7)\\ &= |\langle\psi_j|P_s|\phi\rangle|^2 \ , && (8.8) \end{aligned}$$

where P_s is the projection operator onto $\mathcal{H}$. Let us define the vectors

$$|\chi_j\rangle = P_s|\psi_j\rangle = \sum_{k=0}^{d_s-1}\langle k|\psi_j\rangle|k\rangle \in \mathcal{H}_s \ , \tag{8.9}$$

which are the projections of $\{|\psi_j\rangle\}$ onto $\mathcal{H}_s$, that is, vectors whose components are equal to the first d_s components of the vectors $\{|\psi_j\rangle\}$. Then, the probability (8.8) can be rewritten as

$$p_j = |\langle\chi_j|\phi\rangle|^2 \ . \tag{8.10}$$

Therefore, measuring the state $|\phi\rangle$ with the vectors $\{|\psi_j\rangle\}$ is equivalent to measure with the vectors $|\chi_j\rangle$. Based on that, we will prove that the set of d vectors $|\chi_j\rangle$ defines a POVM.
Analogously to the equation (8.3), we can write the following:

$$\sum_{j=0}^{d-1}\langle k|\chi_j\rangle\langle\chi_j|l\rangle = \sum_{j=0}^{d-1}\left[\left(\sum_{k=0}^{ds-1}\langle k|\psi_j\rangle\langle k|k\rangle\right)\left(\sum_{k=0}^{ds-1}\langle k|\psi_j\rangle^*\langle l|k\rangle^*\right)\right] \tag{8.11}$$

$$= \sum_{j=0}^{d-1}\langle k|\psi_j\rangle\langle\psi_j|l\rangle \tag{8.12}$$

$$= \delta_{kl} \ . \tag{8.13}$$

and see that the completness relation is satisfied. On the other hand, considering that we defined $\{|\chi_j\rangle\} \in \mathcal{H}_s$ with dimension $d_s < d$, where d is the dimension of the extended system $\mathcal{H}$, and noting that the index $j = 0, ..., d-1$ gives d elements, then, we can conclude that the vectors $\{|\chi_j\rangle\}$ form a POVM, with up to d outcomes.

8.2 Experimental Implementation Proposal of a POVM

Using our setup, we can implement experimentally a projective measurement by adding different local phases to each input core of the 7×7 -Multiport Beam Splitter. To do that, it is defined a set of projective measurements formed by the states

$$|\psi_j\rangle = \Phi^{\dagger}\hat{U}^{\dagger}|j\rangle \ , \tag{8.14}$$

where $j = 1, ..., 7$, $\hat{U}$ is the unitary matrix of the multiport and

$$\Phi = \begin{pmatrix} 1 & & & \\ & e^{i\varphi_2} & & \\ & & \ddots & \\ & & & e^{i\varphi_7} \end{pmatrix} \ ,$$

is a diagonal matrix whose elements are the phases applied in each input core of the multiport beam splitter.

We can implement experimentally a finite number of different rank-1 POVM for dimension d_s lower than $d = 7$. This is achived using a sub-set of d_s of the cores as the principal system and the remaining d_a cores as ancilla system [56]. Thereby, the total number of different POVMs is given by:

$$\binom{d}{d_s} = \frac{d!}{d_s!(d-d_s)!} \tag{8.15}$$

since this is the number of combination of d_s elements of a set of d, without repetition. Now taking into account that we can experimentally modify the phase on each core of the system, we have that the rank-1 POVM elements that we can

implement in our experimental setup are $\Pi_j = |\chi_j\rangle\langle\chi_j|$, with

$$|\chi_j\rangle = \bar{\Phi}^{\dagger}_{k_1\cdots k_{d_s}} M_{k_1\cdots k_{d_S}} |j\rangle \ , \tag{8.16}$$

where $k_1 \cdots k_{d_s}$ are the corresponding indices of the cores considered as system, and $\bar{\Phi}_{k_1\cdots k_{d_s}}$ and $M_{k_1\cdots k_{d_S}}$ are the matrices Φ and $U^{\dagger}$, respectively, restricted to the system space. That is, experimentally we can implement a POVM of the finite set of options given by the combinatorial of the cores, and are able to modify the local phase of the cores corresponding to the principal system (see Fig. 8.1). In this work, we will study the particular cases of dimensions $d_s = 3$ and $d_s = 4$.

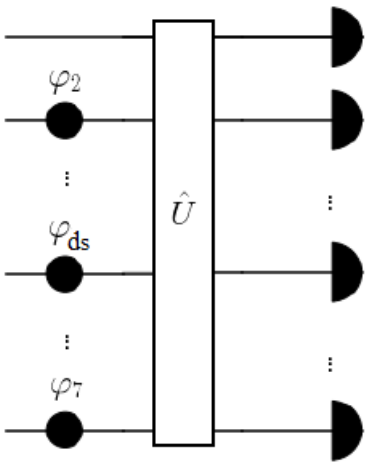

Figure 8.1: Scheme showing a POVM implementation using a 7×7 Multiport Beam Splitter. The horizontal lines represent the fibers, the black circles represent the phase shifts, the box represents the MBS, and the half-circles are detectors. The state is encoded only in the first d_s cores, and each detector is associated with a POVM element.

8.2.0.1 POVMs of $d_s = 3$

For dimension $d_s = 3$, we have 35 different POVMs which can be form by the following matrices $M_{k_1,\ldots k_{d_S}}$:

$$M_{123} = \begin{bmatrix} 0.5639 & 0.2222 & 0.3487 & 0.3929 & 0.3709 & 0.1468 & 0.4444 \\ 0.201 & -0.006542 - 0.1874i & -0.6271 + 0.3102i & 0.332 - 0.01557i & -0.1842 - 0.2868i & 0.3709 - 0.2029i & -0.02196 + 0.1704i \\ 0.3019 & -0.57 + 0.306i & 0.1178 + 0.09943i & -0.162 + 0.295i & -0.1199 - 0.1069i & 0.3572 + 0.09154i & -0.0651 - 0.4328i \end{bmatrix} \tag{8.17}$$

$$M_{124} = \begin{bmatrix} 0.5639 & 0.2222 & 0.3487 & 0.3929 & 0.3709 & 0.1468 & 0.4444 \\ 0.201 & -0.006542 - 0.1874i & -0.6271 + 0.3102i & 0.332 - 0.01557i & -0.1842 - 0.2868i & 0.3709 - 0.2029i & -0.02196 + 0.1704i \\ 0.3749 & 0.3558 + 0.08647i & -0.2245 + 0.2686i & -0.1267 - 0.3353i & -0.02242 + 0.2699i & -0.09359 + 0.4318i & -0.3159 - 0.3254i \end{bmatrix} \tag{8.18}$$

$$M_{125} = \begin{bmatrix} 0.5639 & 0.2222 & 0.3487 & 0.3929 & 0.3709 & 0.1468 & 0.4444 \\ 0.201 & -0.006542 - 0.1874i & -0.6271 + 0.3102i & 0.332 - 0.01557i & -0.1842 - 0.2868i & 0.3709 - 0.2029i & -0.02196 + 0.1704i \\ 0.4918 & -0.1447 - 0.3632i & -0.04691 - 0.1075i & -0.04889 + 0.3414i & 0.02136 + 0.0533i & -0.5262 - 0.3039i & -0.3157 + 0.02007i \end{bmatrix} \tag{8.19}$$

$$M_{126} = \begin{bmatrix} 0.5639 & 0.2222 & 0.3487 & 0.3929 & 0.3709 & 0.1468 & 0.4444 \\ 0.201 & -0.006542 - 0.1874i & -0.6271 + 0.3102i & 0.332 - 0.01557i & -0.1842 - 0.2868i & 0.3709 - 0.2029i & -0.02196 + 0.1704i \\ 0.09054 & 0.2989 + 0.2884i & 0.06289 + 0.2445i & -0.3319 + 0.1445i & -0.01444 - 0.7223i & -0.279 + 0.05535i & 0.08389 + 0.1206i \end{bmatrix} \tag{8.20}$$

$$M_{127} = \begin{bmatrix} 0.5639 & 0.2222 & 0.3487 & 0.3929 & 0.3709 & 0.1468 & 0.4444 \\ 0.201 & -0.006542 - 0.1874i & -0.6271 + 0.3102i & 0.332 - 0.01557i & -0.1842 - 0.2868i & 0.3709 - 0.2029i & -0.02196 + 0.1704i \\ 0.3998 & -0.1033 + 0.1635i & -0.01155 - 0.4061i & -0.3447 - 0.353i & -0.3419 + 0.06981i & 0.1351 - 0.0107i & 0.09887 + 0.4943i \end{bmatrix} \tag{8.21}$$

$$M_{134} = \begin{bmatrix} 0.5639 & 0.2222 & 0.3487 & 0.3929 & 0.3709 & 0.1468 & 0.4444 \\ 0.3019 & -0.57 + 0.306i & 0.1178 + 0.09943i & -0.162 + 0.295i & -0.1199 - 0.1069i & 0.3572 + 0.09154i & -0.0651 - 0.4328i \\ 0.3749 & 0.3558 + 0.08647i & -0.2245 + 0.2686i & -0.1267 - 0.3353i & -0.02242 + 0.2699i & -0.09359 + 0.4318i & -0.3159 - 0.3254i \end{bmatrix} \tag{8.22}$$

$$M_{135} = \begin{bmatrix} 0.5639 & 0.2222 & 0.3487 & 0.3929 & 0.3709 & 0.1468 & 0.4444 \\ 0.3019 & -0.57 + 0.306i & 0.1178 + 0.09943i & -0.162 + 0.295i & -0.1199 - 0.1069i & 0.3572 + 0.09154i & -0.0651 - 0.4328i \\ 0.4918 & -0.1447 - 0.3632i & -0.04691 - 0.1075i & -0.04889 + 0.3414i & 0.02136 + 0.0533i & -0.5262 - 0.3039i & -0.3157 + 0.02007i \end{bmatrix} \tag{8.23}$$

$$M_{136} = \begin{bmatrix} 0.5639 & 0.2222 & 0.3487 & 0.3929 & 0.3709 & 0.1468 & 0.4444 \\ 0.3019 & -0.57 + 0.306i & 0.1178 + 0.09943i & -0.162 + 0.295i & -0.1199 - 0.1069i & 0.3572 + 0.09154i & -0.0651 - 0.4328i \\ 0.09054 & 0.2989 + 0.2884i & 0.06289 + 0.2445i & -0.3319 + 0.1445i & -0.01444 - 0.7223i & -0.279 + 0.05535i & 0.08389 + 0.1206i \end{bmatrix} \tag{8.24}$$

$$M_{137} = \begin{bmatrix} 0.5639 & 0.2222 & 0.3487 & 0.3929 & 0.3709 & 0.1468 & 0.4444 \\ 0.3019 & -0.57 + 0.306\,i & 0.1178 + 0.09943\,i & -0.162 + 0.295\,i & -0.1199 - 0.1069\,i & 0.3572 + 0.09154\,i & -0.0651 - 0.4328\,i \\ 0.3998 & -0.1033 + 0.1635i & -0.01155 - 0.4061i & -0.3447 - 0.353i & -0.3419 + 0.06981i & 0.1351 - 0.01077i & 0.09887 + 0.4943i \end{bmatrix} \tag{8.25}$$

$$M_{145} = \begin{bmatrix} 0.5639 & 0.2222 & 0.3487 & 0.3929 & 0.3709 & 0.1468 & 0.4444 \\ 0.3749 & 0.3558 + 0.08647i & -0.2245 + 0.2686i & -0.1267 - 0.3353i & -0.02242 + 0.2699i & -0.09359 + 0.4318i & -0.3159 - 0.3254i \\ 0.4918 & -0.1447 - 0.3632i & -0.04691 - 0.1075i & -0.04889 + 0.3414i & 0.02136 + 0.0533i & -0.5262 - 0.3039i & -0.3157 + 0.02007i \end{bmatrix} \tag{8.26}$$

$$M_{146} = \begin{bmatrix} 0.5639 & 0.2222 & 0.3487 & 0.3929 & 0.3709 & 0.1468 & 0.4444 \\ 0.3749 & 0.3558 + 0.08647i & -0.2245 + 0.2686i & -0.1267 - 0.3353i & -0.02242 + 0.2699i & -0.09359 + 0.4318i & -0.3159 - 0.3254i \\ 0.09054 & 0.2989 + 0.2884i & 0.06289 + 0.2445i & -0.3319 + 0.1445i & -0.01444 - 0.7223i & -0.279 + 0.05535i & 0.08389 + 0.1206i \end{bmatrix} \tag{8.27}$$

$$M_{147} = \begin{bmatrix} 0.5639 & 0.2222 & 0.3487 & 0.3929 & 0.3709 & 0.1468 & 0.4444 \\ 0.3749 & 0.3558 + 0.08647i & -0.2245 + 0.2686i & -0.1267 - 0.3353i & -0.02242 + 0.2699i & -0.09359 + 0.4318i & -0.3159 - 0.3254i \\ 0.3998 & -0.1033 + 0.1635i & -0.01155 - 0.4061i & -0.3447 - 0.353i & -0.3419 + 0.06981i & 0.1351 - 0.01077i & 0.09887 + 0.4943i \end{bmatrix} \tag{8.28}$$

$$M_{156} = \begin{bmatrix} 0.5639 & 0.2222 & 0.3487 & 0.3929 & 0.3709 & 0.1468 & 0.4444 \\ 0.4918 & -0.1447 - 0.3632i & -0.04691 - 0.1075i & -0.04889 + 0.3414i & 0.02136 + 0.0533i & -0.5262 - 0.3039i & -0.3157 + 0.02007i \\ 0.09054 & 0.2989 + 0.2884i & 0.06289 + 0.2445i & -0.3319 + 0.1445i & -0.01444 - 0.7223i & -0.279 + 0.05535i & 0.08389 + 0.1206i \end{bmatrix} \tag{8.29}$$

$$M_{157} = \begin{bmatrix} 0.5639 & 0.2222 & 0.3487 & 0.3929 & 0.3709 & 0.1468 & 0.4444 \\ 0.4918 & -0.1447 - 0.3632i & -0.04691 - 0.1075i & -0.04889 + 0.3414i & 0.02136 + 0.0533i & -0.5262 - 0.3039i & -0.3157 + 0.02007i \\ 0.3998 & -0.1033 + 0.1635i & -0.01155 - 0.4061i & -0.3447 - 0.353i & -0.3419 + 0.06981i & 0.1351 - 0.01077i & 0.09887 + 0.4943i \end{bmatrix} \tag{8.30}$$

$$M_{167} = \begin{bmatrix} 0.5639 & 0.2222 & 0.3487 & 0.3929 & 0.3709 & 0.1468 & 0.4444 \\ 0.09054 & 0.2989 + 0.2884i & 0.06289 + 0.2445i & -0.3319 + 0.1445i & -0.01444 - 0.7223i & -0.279 + 0.05535i & 0.08389 + 0.1206i \\ 0.3998 & -0.1033 + 0.1635i & -0.01155 - 0.4061i & -0.3447 - 0.353i & -0.3419 + 0.06981i & 0.1351 - 0.01077i & 0.09887 + 0.4943i \end{bmatrix} \tag{8.31}$$

$$M_{267} = \begin{bmatrix} 0.201 & 0.1875 & 0.6997 & 0.3324 & 0.3409 & 0.4227 & 0.1718 \\ 0.09054 & -0.2987 + 0.2887i & 0.05206 - 0.2471i & -0.3383 + 0.1288i & 0.6156 + 0.3782i & -0.2714 - 0.08536i & 0.1089 - 0.09863i \\ 0.3998 & -0.1598 - 0.1089i & -0.1697 + 0.3691i & -0.3278 - 0.3688i & 0.1261 - 0.3254i & 0.1237 + 0.05538i & 0.4776 - 0.1612i \end{bmatrix} \tag{8.32}$$

$$M_{257} = \begin{bmatrix} 0.201 & 0.1875 & 0.6997 & 0.3324 & 0.3409 & 0.4227 & 0.1718 \\ 0.4918 & 0.368 - 0.1319i & -0.005624 + 0.1171i & -0.06483 + 0.3387i & -0.05638 - 0.01083i & -0.3158 - 0.5192i & 0.06025 + 0.3105i \\ 0.3998 & -0.1598 - 0.1089i & -0.1697 + 0.3691i & -0.3278 - 0.3688i & 0.1261 - 0.3254i & 0.1237 + 0.05538i & 0.4776 - 0.1612i \end{bmatrix} \tag{8.33}$$

$$M_{256} = \begin{bmatrix} 0.201 & 0.1875 & 0.6997 & 0.3324 & 0.3409 & 0.4227 & 0.1718 \\ 0.4918 & 0.368 - 0.1319i & -0.005624 + 0.1171i & -0.06483 + 0.3387i & -0.05638 - 0.01083i & -0.3158 - 0.5192i & 0.06025 + 0.3105i \\ 0.09054 & -0.2987 + 0.2887i & 0.05206 - 0.2471i & -0.3383 + 0.1288i & 0.6156 + 0.3782i & -0.2714 - 0.08536i & 0.1089 - 0.09863i \end{bmatrix} \tag{8.34}$$

$$M_{247} = \begin{bmatrix} 0.201 & 0.1875 & 0.6997 & 0.3324 & 0.3409 & 0.4227 & 0.1718 \\ 0.3749 & -0.09883 + 0.3526i & 0.3204 - 0.1412i & -0.1108 - 0.3409i & -0.215 - 0.1647i & -0.2893 + 0.3339i & -0.2824 + 0.3549i \\ 0.3998 & -0.1598 - 0.1089i & -0.1697 + 0.3691i & -0.3278 - 0.3688i & 0.1261 - 0.3254i & 0.1237 + 0.05538i & 0.4776 - 0.1612i \end{bmatrix} \tag{8.35}$$

$$M_{246} = \begin{bmatrix} 0.201 & 0.1875 & 0.6997 & 0.3324 & 0.3409 & 0.4227 & 0.1718 \\ 0.3749 & -0.09883 + 0.3526i & 0.3204 - 0.1412i & -0.1108 - 0.3409i & -0.215 - 0.1647i & -0.2893 + 0.3339i & -0.2824 + 0.3549i \\ 0.09054 & -0.2987 + 0.2887i & 0.05206 - 0.2471i & -0.3383 + 0.1288i & 0.6156 + 0.3782i & -0.2714 - 0.08536i & 0.1089 - 0.09863i \end{bmatrix} \tag{8.36}$$

$$M_{245} = \begin{bmatrix} 0.201 & 0.1875 & 0.6997 & 0.3324 & 0.3409 & 0.4227 & 0.1718 \\ 0.3749 & -0.09883 + 0.3526i & 0.3204 - 0.1412i & -0.1108 - 0.3409i & -0.215 - 0.1647i & -0.2893 + 0.3339i & -0.2824 + 0.3549i \\ 0.4918 & 0.368 - 0.1319i & -0.005624 + 0.1171i & -0.06483 + 0.3387i & -0.05638 - 0.01083i & -0.3158 - 0.5192i & 0.06025 + 0.3105i \end{bmatrix} \tag{8.37}$$

$$M_{237} = \begin{bmatrix} 0.201 & 0.1875 & 0.6997 & 0.3324 & 0.3409 & 0.4227 & 0.1718 \\ 0.3019 & -0.2859 - 0.5804i & -0.0615 - 0.1414i & -0.1756 + 0.2871i & 0.1548 - 0.04311i & 0.2694 + 0.2517i & -0.4209 + 0.1199i \\ 0.3998 & -0.1598 - 0.1089i & -0.1697 + 0.3691i & -0.3278 - 0.3688i & 0.1261 - 0.3254i & 0.1237 + 0.05538i & 0.4776 - 0.1612i \end{bmatrix} \tag{8.38}$$

$$M_{236} = \begin{bmatrix} 0.201 & 0.1875 & 0.6997 & 0.3324 & 0.3409 & 0.4227 & 0.1718 \\ 0.3019 & -0.2859 - 0.5804i & -0.0615 - 0.1414i & -0.1756 + 0.2871i & 0.1548 - 0.04311i & 0.2694 + 0.2517i & -0.4209 + 0.1199i \\ 0.09054 & -0.2987 + 0.2887i & 0.05206 - 0.2471i & -0.3383 + 0.1288i & 0.6156 + 0.3782i & -0.2714 - 0.08536i & 0.1089 - 0.09863i \end{bmatrix} \tag{8.39}$$

$$M_{235} = \begin{bmatrix} 0.201 & 0.1875 & 0.6997 & 0.3324 & 0.3409 & 0.4227 & 0.1718 \\ 0.3019 & -0.2859 - 0.5804i & -0.0615 - 0.1414i & -0.1756 + 0.2871i & 0.1548 - 0.04311i & 0.2694 + 0.2517i & -0.4209 + 0.1199i \\ 0.4918 & 0.368 - 0.1319i & -0.005624 + 0.1171i & -0.06483 + 0.3387i & -0.05638 - 0.01083i & -0.3158 - 0.5192i & 0.06025 + 0.3105i \end{bmatrix} \tag{8.40}$$

$$M_{234} = \begin{bmatrix} 0.201 & 0.1875 & 0.6997 & 0.3324 & 0.3409 & 0.4227 & 0.1718 \\ 0.3019 & -0.2859 - 0.5804i & -0.0615 - 0.1414i & -0.1756 + 0.2871i & 0.1548 - 0.04311i & 0.2694 + 0.2517i & -0.4209 + 0.1199i \\ 0.3749 & -0.09883 + 0.3526i & 0.3204 - 0.1412i & -0.1108 - 0.3409i & -0.215 - 0.1647i & -0.2893 + 0.3339i & -0.2824 + 0.3549i \end{bmatrix} \tag{8.41}$$

$$M_{367} = \begin{bmatrix} 0.3019 & 0.647 & 0.1542 & 0.3365 & 0.1607 & 0.3687 & 0.4377 \\ 0.09054 & -0.1269 - 0.3955i & 0.2058 + 0.1463i & 0.2864 + 0.2213i & 0.4915 + 0.5295i & -0.2566 + 0.1229i & -0.1318 + 0.06502i \\ 0.3998 & 0.1683 - 0.09526i & -0.2707 - 0.3029i & -0.1435 + 0.4721i & 0.2088 - 0.2797i & 0.1282 - 0.04397i & -0.5035 + 0.02425i \end{bmatrix} \tag{8.42}$$

$$M_{357} = \begin{bmatrix} 0.3019 & 0.647 & 0.1542 & 0.3365 & 0.1607 & 0.3687 & 0.4377 \\ 0.4918 & -0.0443 + 0.3884i & -0.1052 - 0.05189i & 0.3228 - 0.1215i & -0.05141 - 0.02556i & -0.5852 - 0.1638i & 0.02711 - 0.3152i \\ 0.3998 & 0.1683 - 0.09526i & -0.2707 - 0.3029i & -0.1435 + 0.4721i & 0.2088 - 0.2797i & 0.1282 - 0.04397i & -0.5035 + 0.02425i \end{bmatrix} \tag{8.43}$$

$$M_{356} = \begin{bmatrix} 0.3019 & 0.647 & 0.1542 & 0.3365 & 0.1607 & 0.3687 & 0.4377 \\ 0.4918 & -0.0443 + 0.3884i & -0.1052 - 0.05189i & 0.3228 - 0.1215i & -0.05141 - 0.02556i & -0.5852 - 0.1638i & 0.02711 - 0.3152i \\ 0.09054 & -0.1269 - 0.3955i & 0.2058 + 0.1463i & 0.2864 + 0.2213i & 0.4915 + 0.5295i & -0.2566 + 0.1229i & -0.1318 + 0.06502i \end{bmatrix} \tag{8.44}$$

$$M_{347} = \begin{bmatrix} 0.3019 & 0.647 & 0.1542 & 0.3365 & 0.1607 & 0.3687 & 0.4377 \\ 0.3749 & -0.2726 - 0.2445i & 0.001653 + 0.3501i & -0.2329 + 0.2725i & -0.1629 - 0.2164i & 0.01653 + 0.4415i & 0.3688 - 0.264i \\ 0.3998 & 0.1683 - 0.09526i & -0.2707 - 0.3029i & -0.1435 + 0.4721i & 0.2088 - 0.2797i & 0.1282 - 0.04397i & -0.5035 + 0.02425i \end{bmatrix} \tag{8.45}$$

$$M_{346} = \begin{bmatrix} 0.3019 & 0.647 & 0.1542 & 0.3365 & 0.1607 & 0.3687 & 0.4377 \\ 0.3749 & -0.2726 - 0.2445i & 0.001653 + 0.3501i & -0.2329 + 0.2725i & -0.1629 - 0.2164i & 0.01653 + 0.4415i & 0.3688 - 0.264i \\ 0.09054 & -0.1269 - 0.3955i & 0.2058 + 0.1463i & 0.2864 + 0.2213i & 0.4915 + 0.5295i & -0.2566 + 0.1229i & -0.1318 + 0.06502i \end{bmatrix} \tag{8.46}$$

$$M_{345} = \begin{bmatrix} 0.3019 & 0.647 & 0.1542 & 0.3365 & 0.1607 & 0.3687 & 0.4377 \\ 0.3749 & -0.2726 - 0.2445i & 0.001653 + 0.3501i & -0.2329 + 0.2725i & -0.1629 - 0.2164i & 0.01653 + 0.4415i & 0.3688 - 0.264i \\ 0.4918 & -0.0443 + 0.3884i & -0.1052 - 0.05189i & 0.3228 - 0.1215i & -0.05141 - 0.02556i & -0.5852 - 0.1638i & 0.02711 - 0.3152i \end{bmatrix} \tag{8.47}$$

$$M_{456} = \begin{bmatrix} 0.3749 & 0.3662 & 0.3501 & 0.3584 & 0.2709 & 0.4418 & 0.4535 \\ 0.4918 & -0.2263 - 0.3188i & -0.05239 + 0.1049i & -0.3021 - 0.1664i & 0.05134 - 0.02569i & -0.1856 + 0.5787i & 0.2055 - 0.2405i \\ 0.09054 & 0.3586 + 0.2097i & 0.1473 - 0.2051i & -0.01789 - 0.3615i & -0.7187 + 0.07419i & 0.1132 + 0.261i & -0.145 - 0.02382i \end{bmatrix} \tag{8.48}$$

$$M_{457} = \begin{bmatrix} 0.3749 & 0.3662 & 0.3501 & 0.3584 & 0.2709 & 0.4418 & 0.4535 \\ 0.4918 & -0.2263 - 0.3188i & -0.05239 + 0.1049i & -0.3021 - 0.1664i & 0.05134 - 0.02569i & -0.1856 + 0.5787i & 0.2055 - 0.2405i \\ 0.3998 & -0.06171 + 0.1833i & -0.3041 + 0.2693i & 0.4521 - 0.1977i & 0.09788 + 0.335i & -0.03915 - 0.1297i & -0.4235 - 0.2733i \end{bmatrix} \tag{8.49}$$

$$M_{467} = \begin{bmatrix} 0.3749 & 0.3662 & 0.3501 & 0.3584 & 0.2709 & 0.4418 & 0.4535 \\ 0.09054 & 0.3586 + 0.2097i & 0.1473 - 0.2051i & -0.01789 - 0.3615i & -0.7187 + 0.07419i & 0.1132 + 0.261i & -0.145 - 0.02382i \\ 0.3998 & -0.06171 + 0.1833i & -0.3041 + 0.2693i & 0.4521 - 0.1977i & 0.09788 + 0.335i & -0.03915 - 0.1297i & -0.4235 - 0.2733i \end{bmatrix} \tag{8.50}$$

$$M_{567} = \begin{bmatrix} 0.4918 & 0.3909 & 0.1173 & 0.3449 & 0.05741 & 0.6077 & 0.3163 \\ 0.09054 & -0.3786 + 0.171i & -0.2493 - 0.04015i & 0.1901 + 0.308i & -0.6759 - 0.2553i & 0.214 - 0.1875i & -0.07607 - 0.1257i \\ 0.3998 & -0.1137 - 0.1564i & 0.3768 + 0.1518i & -0.3006 + 0.3913i & -0.06239 + 0.3434i & -0.1116 + 0.0769i & -0.06731 - 0.4996i \end{bmatrix} \tag{8.51}$$

8.2.0.2 POVMs of $d_s = 4$

For dimension $d_s = 4$, we also have 35 different POVMs which can be form by the following matrices $M_{k_1,\ldots k_{d_S}}$:

$$M_{1234} = \begin{bmatrix} 0.5639 & 0.2222 & 0.3487 & 0.3929 & 0.3709 & 0.1468 & 0.4444 \\ 0.201 & -0.006542 - 0.1874i & -0.6271 + 0.3102i & 0.332 - 0.01557i & -0.1842 - 0.2868i & 0.3709 - 0.2029i & -0.02196 + 0.1704i \\ 0.3019 & -0.57 + 0.306i & 0.1178 + 0.09943i & -0.162 + 0.295i & -0.1199 - 0.1069i & 0.3572 + 0.09154i & -0.0651 - 0.4328i \\ 0.3749 & 0.3558 + 0.08647i & -0.2245 + 0.2686i & -0.1267 - 0.3353i & -0.02242 + 0.2699i & -0.09359 + 0.4318i & -0.3159 - 0.3254i \end{bmatrix} \tag{8.52}$$

$$M_{1235} = \begin{bmatrix} 0.5639 & 0.2222 & 0.3487 & 0.3929 & 0.3709 & 0.1468 & 0.4444 \\ 0.201 & -0.006542 - 0.1874i & -0.6271 + 0.3102i & 0.332 - 0.01557i & -0.1842 - 0.2868i & 0.3709 - 0.2029i & -0.02196 + 0.1704i \\ 0.3019 & -0.57 + 0.306i & 0.1178 + 0.09943i & -0.162 + 0.295i & -0.1199 - 0.1069i & 0.3572 + 0.09154i & -0.0651 - 0.4328i \\ 0.4918 & -0.1447 - 0.3632i & -0.04691 - 0.1075i & -0.04889 + 0.3414i & 0.02136 + 0.0533i & -0.5262 - 0.3039i & -0.3157 + 0.02007i \end{bmatrix} \tag{8.53}$$

$$M_{1236} = \begin{bmatrix} 0.5639 & 0.2222 & 0.3487 & 0.3929 & 0.3709 & 0.1468 & 0.4444 \\ 0.201 & -0.006542 - 0.1874i & -0.6271 + 0.3102i & 0.332 - 0.01557i & -0.1842 - 0.2868i & 0.3709 - 0.2029i & -0.02196 + 0.1704i \\ 0.3019 & -0.57 + 0.306i & 0.1178 + 0.09943i & -0.162 + 0.295i & -0.1199 - 0.1069i & 0.3572 + 0.09154i & -0.0651 - 0.4328i \\ 0.09054 & 0.2989 + 0.2884i & 0.06289 + 0.2445i & -0.3319 + 0.1445i & -0.01444 - 0.7223i & -0.279 + 0.05535i & 0.08389 + 0.1206i \end{bmatrix} \tag{8.54}$$

$$M_{1237} = \begin{bmatrix} 0.5639 & 0.2222 & 0.3487 & 0.3929 & 0.3709 & 0.1468 & 0.4444 \\ 0.201 & -0.006542 - 0.1874i & -0.6271 + 0.3102i & 0.332 - 0.01557i & -0.1842 - 0.2868i & 0.3709 - 0.2029i & -0.02196 + 0.1704i \\ 0.3019 & -0.57 + 0.306i & 0.1178 + 0.09943i & -0.162 + 0.295i & -0.1199 - 0.1069i & 0.3572 + 0.09154i & -0.0651 - 0.4328i \\ 0.3998 & -0.1033 + 0.1635i & -0.01155 - 0.4061i & -0.3447 - 0.353i & -0.3419 + 0.06981i & 0.1351 - 0.01077i & 0.09887 + 0.4943i \end{bmatrix} \tag{8.55}$$

$$M_{1245} = \begin{bmatrix} 0.5639 & 0.2222 & 0.3487 & 0.3929 & 0.3709 & 0.1468 & 0.4444 \\ 0.201 & -0.006542 - 0.1874i & -0.6271 + 0.3102i & 0.332 - 0.01557i & -0.1842 - 0.2868i & 0.3709 - 0.2029i & -0.02196 + 0.1704i \\ 0.3749 & 0.3558 + 0.08647i & -0.2245 + 0.2686i & -0.1267 - 0.3353i & -0.02242 + 0.2699i & -0.09359 + 0.4318i & -0.3159 - 0.3254i \\ 0.4918 & -0.1447 - 0.3632i & -0.04691 - 0.1075i & -0.04889 + 0.3414i & 0.02136 + 0.0533i & -0.5262 - 0.3039i & -0.3157 + 0.02007i \end{bmatrix} \tag{8.56}$$

$$M_{1246} = \begin{bmatrix} 0.5639 & 0.2222 & 0.3487 & 0.3929 & 0.3709 & 0.1468 & 0.4444 \\ 0.201 & -0.006542 - 0.1874i & -0.6271 + 0.3102i & 0.332 - 0.01557i & -0.1842 - 0.2868i & 0.3709 - 0.2029i & -0.02196 + 0.1704i \\ 0.3749 & 0.3558 + 0.08647i & -0.2245 + 0.2686i & -0.1267 - 0.3353i & -0.02242 + 0.2699i & -0.09359 + 0.4318i & -0.3159 - 0.3254i \\ 0.09054 & 0.2989 + 0.2884i & 0.06289 + 0.2445i & -0.3319 + 0.1445i & -0.01444 - 0.7223i & -0.279 + 0.05535i & 0.08389 + 0.1206i \end{bmatrix} \tag{8.57}$$

$$M_{1247} = \begin{bmatrix} 0.5639 & 0.2222 & 0.3487 & 0.3929 & 0.3709 & 0.1468 & 0.4444 \\ 0.201 & -0.006542 - 0.1874i & -0.6271 + 0.3102i & 0.332 - 0.01557i & -0.1842 - 0.2868i & 0.3709 - 0.2029i & -0.02196 + 0.1704i \\ 0.3749 & 0.3558 + 0.08647i & -0.2245 + 0.2686i & -0.1267 - 0.3353i & -0.02242 + 0.2699i & -0.09359 + 0.4318i & -0.3159 - 0.3254i \\ 0.3998 & -0.1033 + 0.1635i & -0.01155 - 0.4061i & -0.3447 - 0.353i & -0.3419 + 0.06981i & 0.1351 - 0.01077i & 0.09887 + 0.4943i \end{bmatrix} \tag{8.58}$$

$$M_{1256} = \begin{bmatrix} 0.5639 & 0.2222 & 0.3487 & 0.3929 & 0.3709 & 0.1468 & 0.4444 \\ 0.201 & -0.006542 - 0.1874i & -0.6271 + 0.3102i & 0.332 - 0.01557i & -0.1842 - 0.2868i & 0.3709 - 0.2029i & -0.02196 + 0.1704i \\ 0.4918 & -0.1447 - 0.3632i & -0.04691 - 0.1075i & -0.04889 + 0.3414i & 0.02136 + 0.0533i & -0.5262 - 0.3039i & -0.3157 + 0.02007i \\ 0.09054 & 0.2989 + 0.2884i & 0.06289 + 0.2445i & -0.3319 + 0.1445i & -0.01444 - 0.7223i & -0.279 + 0.05535i & 0.08389 + 0.1206i \end{bmatrix} \tag{8.59}$$

$$M_{1257} = \begin{bmatrix} 0.5639 & 0.2222 & 0.3487 & 0.3929 & 0.3709 & 0.1468 & 0.4444 \\ 0.201 & -0.006542 - 0.1874i & -0.6271 + 0.3102i & 0.332 - 0.01557i & -0.1842 - 0.2868i & 0.3709 - 0.2029i & -0.02196 + 0.1704i \\ 0.4918 & -0.1447 - 0.3632i & -0.04691 - 0.1075i & -0.04889 + 0.3414i & 0.02136 + 0.0533i & -0.5262 - 0.3039i & -0.3157 + 0.02007i \\ 0.3998 & -0.1033 + 0.1635i & -0.01155 - 0.4061i & -0.3447 - 0.353i & -0.3419 + 0.06981i & 0.1351 - 0.01077i & 0.09887 + 0.4943i \end{bmatrix} \tag{8.60}$$

$$M_{1267} = \begin{bmatrix} 0.5639 & 0.2222 & 0.3487 & 0.3929 & 0.3709 & 0.1468 & 0.4444 \\ 0.201 & -0.006542 - 0.1874i & -0.6271 + 0.3102i & 0.332 - 0.01557i & -0.1842 - 0.2868i & 0.3709 - 0.2029i & -0.02196 + 0.1704i \\ 0.09054 & 0.2989 + 0.2884i & 0.06289 + 0.2445i & -0.3319 + 0.1445i & -0.01444 - 0.7223i & -0.279 + 0.05535i & 0.08389 + 0.1206i \\ 0.3998 & -0.1033 + 0.1635i & -0.01155 - 0.4061i & -0.3447 - 0.353i & -0.3419 + 0.06981i & 0.1351 - 0.01077i & 0.09887 + 0.4943i \end{bmatrix} \tag{8.61}$$

$$M_{1345} = \begin{bmatrix} 0.5639 & 0.2222 & 0.3487 & 0.3929 & 0.3709 & 0.1468 & 0.4444 \\ 0.3019 & -0.57 + 0.306i & 0.1178 + 0.09943i & -0.162 + 0.295i & -0.1199 - 0.1069i & 0.3572 + 0.09154i & -0.0651 - 0.4328i \\ 0.3749 & 0.3558 + 0.08647i & -0.2245 + 0.2686i & -0.1267 - 0.3353i & -0.02242 + 0.2699i & -0.09359 + 0.4318i & -0.3159 - 0.3254i \\ 0.4918 & -0.1447 - 0.3632i & -0.04691 - 0.1075i & -0.04889 + 0.3414i & 0.02136 + 0.0533i & -0.5262 - 0.3039i & -0.3157 + 0.02007i \end{bmatrix} \tag{8.62}$$

$$M_{1346} = \begin{bmatrix} 0.5639 & 0.2222 & 0.3487 & 0.3929 & 0.3709 & 0.1468 & 0.4444 \\ 0.3019 & -0.57 + 0.306i & 0.1178 + 0.09943i & -0.162 + 0.295i & -0.1199 - 0.1069i & 0.3572 + 0.09154i & -0.0651 - 0.4328i \\ 0.3749 & 0.3558 + 0.08647i & -0.2245 + 0.2686i & -0.1267 - 0.3353i & -0.02242 + 0.2699i & -0.09359 + 0.4318i & -0.3159 - 0.3254i \\ 0.09054 & 0.2989 + 0.2884i & 0.06289 + 0.2445i & -0.3319 + 0.1445i & -0.01444 - 0.7223i & -0.279 + 0.05535i & 0.08389 + 0.1206i \end{bmatrix} \tag{8.63}$$

$$M_{1347} = \begin{bmatrix} 0.5639 & 0.2222 & 0.3487 & 0.3929 & 0.3709 & 0.1468 & 0.4444 \\ 0.3019 & -0.57 + 0.306i & 0.1178 + 0.09943i & -0.162 + 0.295i & -0.1199 - 0.1069i & 0.3572 + 0.09154i & -0.0651 - 0.4328i \\ 0.3749 & 0.3558 + 0.08647i & -0.2245 + 0.2686i & -0.1267 - 0.3353i & -0.02242 + 0.2699i & -0.09359 + 0.4318i & -0.3159 - 0.3254i \\ 0.3998 & -0.1033 + 0.1635i & -0.01155 - 0.4061i & -0.3447 - 0.353i & -0.3419 + 0.06981i & 0.1351 - 0.01077i & 0.09887 + 0.4943i \end{bmatrix} \tag{8.64}$$

$$M_{1356} = \begin{bmatrix} 0.5639 & 0.2222 & 0.3487 & 0.3929 & 0.3709 & 0.1468 & 0.4444 \\ 0.3019 & -0.57 + 0.306i & 0.1178 + 0.09943i & -0.162 + 0.295i & -0.1199 - 0.1069i & 0.3572 + 0.09154i & -0.0651 - 0.4328i \\ 0.4918 & -0.1447 - 0.3632i & -0.04691 - 0.1075i & -0.04889 + 0.3414i & 0.02136 + 0.0533i & -0.5262 - 0.3039i & -0.3157 + 0.02007i \\ 0.09054 & 0.2989 + 0.2884i & 0.06289 + 0.2445i & -0.3319 + 0.1445i & -0.01444 - 0.7223i & -0.279 + 0.05535i & 0.08389 + 0.1206i \end{bmatrix} \tag{8.65}$$

$$M_{1357} = \begin{bmatrix} 0.5639 & 0.2222 & 0.3487 & 0.3929 & 0.3709 & 0.1468 & 0.4444 \\ 0.3019 & -0.57 + 0.306i & 0.1178 + 0.09943i & -0.162 + 0.295mathrmi & -0.1199 - 0.1069i & 0.3572 + 0.09154i & -0.0651 - 0.4328i \\ 0.4918 & -0.1447 - 0.3632i & -0.04691 - 0.1075i & -0.04889 + 0.3414i & 0.02136 + 0.0533i & -0.5262 - 0.3039i & -0.3157 + 0.02007i \\ 0.3998 & -0.1033 + 0.1635i & -0.01155 - 0.4061i & -0.3447 - 0.353i & -0.3419 + 0.06981i & 0.1351 - 0.01077i & 0.09887 + 0.4943i \end{bmatrix} \tag{8.66}$$

$$M_{1367} = \begin{bmatrix} 0.5639 & 0.2222 & 0.3487 & 0.3929 & 0.3709 & 0.1468 & 0.4444 \\ 0.3019 & -0.57 + 0.306i & 0.1178 + 0.09943i & -0.162 + 0.295i & -0.1199 - 0.1069i & 0.3572 + 0.09154i & -0.0651 - 0.4328i \\ 0.09054 & 0.2989 + 0.2884i & 0.06289 + 0.2445i & -0.3319 + 0.1445i & -0.01444 - 0.7223i & -0.279 + 0.05535i & 0.08389 + 0.1206i \\ 0.3998 & -0.1033 + 0.1635i & -0.01155 - 0.4061i & -0.3447 - 0.353i & -0.3419 + 0.06981i & 0.1351 - 0.01077i & 0.09887 + 0.4943i \end{bmatrix} \tag{8.67}$$

$$M_{1456} = \begin{bmatrix} 0.5639 & 0.2222 & 0.3487 & 0.3929 & 0.3709 & 0.1468 & 0.4444 \\ 0.3749 & 0.3558 + 0.08647i & -0.2245 + 0.2686i & -0.1267 - 0.3353i & -0.02242 + 0.2699i & -0.09359 + 0.4318i & -0.3159 - 0.3254i \\ 0.4918 & -0.1447 - 0.3632i & -0.04691 - 0.1075i & -0.04889 + 0.3414i & 0.02136 + 0.0533i & -0.5262 - 0.3039i & -0.3157 + 0.02007i \\ 0.09054 & 0.2989 + 0.2884i & 0.06289 + 0.2445i & -0.3319 + 0.1445i & -0.01444 - 0.7223i & -0.279 + 0.05535i & 0.08389 + 0.1206i \end{bmatrix} \tag{8.68}$$

$$M_{1457} = \begin{bmatrix} 0.5639 & 0.2222 & 0.3487 & 0.3929 & 0.3709 & 0.1468 & 0.4444 \\ 0.3749 & 0.3558 + 0.08647i & -0.2245 + 0.2686i & -0.1267 - 0.3353i & -0.02242 + 0.2699i & -0.09359 + 0.4318i & -0.3159 - 0.3254i \\ 0.4918 & -0.1447 - 0.3632i & -0.04691 - 0.1075i & -0.04889 + 0.3414i & 0.02136 + 0.0533i & -0.5262 - 0.3039i & -0.3157 + 0.02007i \\ 0.3998 & -0.1033 + 0.1635i & -0.01155 - 0.4061i & -0.3447 - 0.353i & -0.3419 + 0.06981i & 0.1351 - 0.01077i & 0.09887 + 0.4943i \end{bmatrix} \tag{8.69}$$

$$M_{1467} = \begin{bmatrix} 0.5639 & 0.2222 & 0.3487 & 0.3929 & 0.3709 & 0.1468 & 0.4444 \\ 0.3749 & 0.3558 + 0.08647i & -0.2245 + 0.2686i & -0.1267 - 0.3353i & -0.02242 + 0.2699i & -0.09359 + 0.4318i & -0.3159 - 0.3254i \\ 0.09054 & 0.2989 + 0.2884i & 0.06289 + 0.2445i & -0.3319 + 0.1445i & -0.01444 - 0.7223i & -0.279 + 0.05535i & 0.08389 + 0.1206i \\ 0.3998 & -0.1033 + 0.1635i & -0.01155 - 0.4061i & -0.3447 - 0.353i & -0.3419 + 0.06981i & 0.1351 - 0.01077i & 0.09887 + 0.4943i \end{bmatrix} \tag{8.70}$$

$$M_{1567} = \begin{bmatrix} 0.5639 & 0.2222 & 0.3487 & 0.3929 & 0.3709 & 0.1468 & 0.4444 \\ 0.4918 & -0.1447 - 0.3632i & -0.04691 - 0.1075i & -0.04889 + 0.3414i & 0.02136 + 0.0533i & -0.5262 - 0.3039i & -0.3157 + 0.02007i \\ 0.09054 & 0.2989 + 0.2884i & 0.06289 + 0.2445i & -0.3319 + 0.1445i & -0.01444 - 0.7223i & -0.279 + 0.05535i & 0.08389 + 0.1206i \\ 0.3998 & -0.1033 + 0.1635i & -0.01155 - 0.4061i & -0.3447 - 0.353i & -0.3419 + 0.06981i & 0.1351 - 0.01077i & 0.09887 + 0.4943i \end{bmatrix} \tag{8.71}$$

$$M_{2345} = \begin{bmatrix} 0.201 & 0.1875 & 0.6997 & 0.3324 & 0.3409 & 0.4227 & 0.1718 \\ 0.3019 & -0.2859 - 0.5804i & -0.0615 - 0.1414i & -0.1756 + 0.2871i & 0.1548 - 0.04311i & 0.2694 + 0.2517i & -0.4209 + 0.1199i \\ 0.3749 & -0.09883 + 0.3526i & 0.3204 - 0.1412i & -0.1108 - 0.3409i & -0.215 - 0.1647i & -0.2893 + 0.3339i & -0.2824 + 0.3549i \\ 0.4918 & 0.368 - 0.1319i & -0.005624 + 0.1171i & -0.06483 + 0.3387i & -0.05638 - 0.01083i & -0.3158 - 0.5192i & 0.06025 + 0.3105i \end{bmatrix} \tag{8.72}$$

$$M_{2346} = \begin{bmatrix} 0.201 & 0.1875 & 0.6997 & 0.3324 & 0.3409 & 0.4227 & 0.1718 \\ 0.3019 & -0.2859 - 0.5804i & -0.0615 - 0.1414i & -0.1756 + 0.2871i & 0.1548 - 0.04311i & 0.2694 + 0.2517i & -0.4209 + 0.1199i \\ 0.3749 & -0.09883 + 0.3526i & 0.3204 - 0.1412i & -0.1108 - 0.3409i & -0.215 - 0.1647i & -0.2893 + 0.3339i & -0.2824 + 0.3549i \\ 0.09054 & -0.2987 + 0.2887i & 0.05206 - 0.2471i & -0.3383 + 0.1288i & 0.6156 + 0.3782i & -0.2714 - 0.08536i & 0.1089 - 0.09863i \end{bmatrix} \tag{8.73}$$

$$M_{2347} = \begin{bmatrix} 0.201 & 0.1875 & 0.6997 & 0.3324 & 0.3409 & 0.4227 & 0.1718 \\ 0.3019 & -0.2859 - 0.5804i & -0.0615 - 0.1414i & -0.1756 + 0.2871i & 0.1548 - 0.04311i & 0.2694 + 0.2517i & -0.4209 + 0.1199i \\ 0.3749 & -0.09883 + 0.3526i & 0.3204 - 0.1412i & -0.1108 - 0.3409i & -0.215 - 0.1647i & -0.2893 + 0.3339i & -0.2824 + 0.3549i \\ 0.3998 & -0.1598 - 0.1089i & -0.1697 + 0.3691i & -0.3278 - 0.3688i & 0.1261 - 0.3254i & 0.1237 + 0.05538i & 0.4776 - 0.1612i \end{bmatrix} \tag{8.74}$$

$$M_{2356} = \begin{bmatrix} 0.201 & 0.1875 & 0.6997 & 0.3324 & 0.3409 & 0.4227 & 0.1718 \\ 0.3019 & -0.2859 - 0.5804i & -0.0615 - 0.1414i & -0.1756 + 0.2871i & 0.1548 - 0.04311i & 0.2694 + 0.2517i & -0.4209 + 0.1199i \\ 0.4918 & 0.368 - 0.1319i & -0.005624 + 0.1171i & -0.06483 + 0.3387i & -0.05638 - 0.01083i & -0.3158 - 0.5192i & 0.06025 + 0.3105i \\ 0.09054 & -0.2987 + 0.2887i & 0.05206 - 0.2471i & -0.3383 + 0.1288i & 0.6156 + 0.3782i & -0.2714 - 0.08536i & 0.1089 - 0.09863i \end{bmatrix} \tag{8.75}$$

$$M_{2357} = \begin{bmatrix} 0.201 & 0.1875 & 0.6997 & 0.3324 & 0.3409 & 0.4227 & 0.1718 \\ 0.3019 & -0.2859 - 0.5804i & -0.0615 - 0.1414i & -0.1756 + 0.2871i & 0.1548 - 0.04311i & 0.2694 + 0.2517i & -0.4209 + 0.1199i \\ 0.4918 & 0.368 - 0.1319i & -0.005624 + 0.1171i & -0.06483 + 0.3387i & -0.05638 - 0.01083i & -0.3158 - 0.5192i & 0.06025 + 0.3105i \\ 0.3998 & -0.1598 - 0.1089i & -0.1697 + 0.3691i & -0.3278 - 0.3688i & 0.1261 - 0.3254i & 0.1237 + 0.05538i & 0.4776 - 0.1612i \end{bmatrix} \tag{8.76}$$

$$M_{2367} = \begin{bmatrix} 0.201 & 0.1875 & 0.6997 & 0.3324 & 0.3409 & 0.4227 & 0.1718 \\ 0.3019 & -0.2859 - 0.5804i & -0.0615 - 0.1414i & -0.1756 + 0.2871i & 0.1548 - 0.04311i & 0.2694 + 0.2517i & -0.4209 + 0.1199i \\ 0.09054 & -0.2987 + 0.2887i & 0.05206 - 0.2471i & -0.3383 + 0.1288i & 0.6156 + 0.3782i & -0.2714 - 0.08536i & 0.1089 - 0.09863i \\ 0.3998 & -0.1598 - 0.1089i & -0.1697 + 0.3691i & -0.3278 - 0.3688i & 0.1261 - 0.3254i & 0.1237 + 0.05538i & 0.4776 - 0.1612i \end{bmatrix} \tag{8.77}$$

$$M_{2456} = \begin{bmatrix} 0.201 & 0.1875 & 0.6997 & 0.3324 & 0.3409 & 0.4227 & 0.1718 \\ 0.3749 & -0.09883 + 0.3526i & 0.3204 - 0.1412i & -0.1108 - 0.3409i & -0.215 - 0.1647i & -0.2893 + 0.3339i & -0.2824 + 0.3549i \\ 0.4918 & 0.368 - 0.1319i & -0.005624 + 0.1171i & -0.06483 + 0.3387i & -0.05638 - 0.01083i & -0.3158 - 0.5192i & 0.06025 + 0.3105i \\ 0.09054 & -0.2987 + 0.2887i & 0.05206 - 0.2471i & -0.3383 + 0.1288i & 0.6156 + 0.3782i & -0.2714 - 0.08536i & 0.1089 - 0.09863i \end{bmatrix} \tag{8.78}$$

$$M_{2457} = \begin{bmatrix} 0.201 & 0.1875 & 0.6997 & 0.3324 & 0.3409 & 0.4227 & 0.1718 \\ 0.3749 & -0.09883 + 0.3526i & 0.3204 - 0.1412i & -0.1108 - 0.3409i & -0.215 - 0.1647i & -0.2893 + 0.3339i & -0.2824 + 0.3549i \\ 0.4918 & 0.368 - 0.1319i & -0.005624 + 0.1171i & -0.06483 + 0.3387i & -0.05638 - 0.01083i & -0.3158 - 0.5192i & 0.06025 + 0.3105i \\ 0.3998 & -0.1598 - 0.1089i & -0.1697 + 0.3691i & -0.3278 - 0.3688i & 0.1261 - 0.3254i & 0.1237 + 0.05538i & 0.4776 - 0.1612i \end{bmatrix} \tag{8.79}$$

$$M_{2467} = \begin{bmatrix} 0.201 & 0.1875 & 0.6997 & 0.3324 & 0.3409 & 0.4227 & 0.1718 \\ 0.3749 & -0.09883 + 0.3526i & 0.3204 - 0.1412i & -0.1108 - 0.3409i & -0.215 - 0.1647i & -0.2893 + 0.3339i & -0.2824 + 0.3549i \\ 0.09054 & -0.2987 + 0.2887i & 0.05206 - 0.2471i & -0.3383 + 0.1288i & 0.6156 + 0.3782i & -0.2714 - 0.08536i & 0.1089 - 0.09863i \\ 0.3998 & -0.1598 - 0.1089i & -0.1697 + 0.3691i & -0.3278 - 0.3688i & 0.1261 - 0.3254i & 0.1237 + 0.05538i & 0.4776 - 0.1612i \end{bmatrix} \tag{8.80}$$

$$M_{2567} = \begin{bmatrix} 0.201 & 0.1875 & 0.6997 & 0.3324 & 0.3409 & 0.4227 & 0.1718 \\ 0.4918 & 0.368 - 0.1319i & -0.005624 + 0.1171i & -0.06483 + 0.3387i & -0.05638 - 0.01083i & -0.3158 - 0.5192i & 0.06025 + 0.3105i \\ 0.09054 & -0.2987 + 0.2887i & 0.05206 - 0.2471i & -0.3383 + 0.1288i & 0.6156 + 0.3782i & -0.2714 - 0.08536i & 0.1089 - 0.09863i \\ 0.3998 & -0.1598 - 0.1089i & -0.1697 + 0.3691i & -0.3278 - 0.3688i & 0.1261 - 0.3254i & 0.1237 + 0.05538i & 0.4776 - 0.1612i \end{bmatrix} \tag{8.81}$$

$$M_{3456} = \begin{bmatrix} 0.3019 & 0.647 & 0.1542 & 0.3365 & 0.1607 & 0.3687 & 0.4377 \\ 0.3749 & -0.2726 - 0.2445i & 0.001653 + 0.3501i & -0.2329 + 0.2725i & -0.1629 - 0.2164i & 0.01653 + 0.4415i & 0.3688 - 0.264i \\ 0.4918 & -0.0443 + 0.3884i & -0.1052 - 0.05189i & 0.3228 - 0.1215i & -0.05141 - 0.02556i & -0.5852 - 0.1638i & 0.02711 - 0.3152i \\ 0.09054 & -0.1269 - 0.3955i & 0.2058 + 0.1463i & 0.2864 + 0.2213i & 0.4915 + 0.5295i & -0.2566 + 0.1229i & -0.1318 + 0.06502i \end{bmatrix} \tag{8.82}$$

$$M_{3457} = \begin{bmatrix} 0.3019 & 0.647 & 0.1542 & 0.3365 & 0.1607 & 0.3687 & 0.4377 \\ 0.3749 & -0.2726 - 0.2445i & 0.001653 + 0.3501i & -0.2329 + 0.2725i & -0.1629 - 0.2164i & 0.01653 + 0.4415i & 0.3688 - 0.264i \\ 0.4918 & -0.0443 + 0.3884i & -0.1052 - 0.05189i & 0.3228 - 0.1215i & -0.05141 - 0.02556i & -0.5852 - 0.1638i & 0.02711 - 0.3152i \\ 0.3998 & 0.1683 - 0.09526i & -0.2707 - 0.3029i & -0.1435 + 0.4721i & 0.2088 - 0.2797i & 0.1282 - 0.04397i & -0.5035 + 0.02425i \end{bmatrix} \tag{8.83}$$

$$M_{3467} = \begin{bmatrix} 0.3019 & 0.647 & 0.1542 & 0.3365 & 0.1607 & 0.3687 & 0.4377 \\ 0.3749 & -0.2726 - 0.2445i & 0.001653 + 0.3501i & -0.2329 + 0.2725i & -0.1629 - 0.2164i & 0.01653 + 0.4415i & 0.3688 - 0.264i \\ 0.09054 & -0.1269 - 0.3955i & 0.2058 + 0.1463i & 0.2864 + 0.2213i & 0.4915 + 0.5295i & -0.2566 + 0.1229i & -0.1318 + 0.06502i \\ 0.3998 & 0.1683 - 0.09526i & -0.2707 - 0.3029i & -0.1435 + 0.4721i & 0.2088 - 0.2797i & 0.1282 - 0.04397i & -0.5035 + 0.02425i \end{bmatrix} \tag{8.84}$$

$$M_{3567} = \begin{bmatrix} 0.3019 & 0.647 & 0.1542 & 0.3365 & 0.1607 & 0.3687 & 0.4377 \\ 0.4918 & -0.0443 + 0.3884i & -0.1052 - 0.05189i & 0.3228 - 0.1215i & -0.05141 - 0.02556i & -0.5852 - 0.1638i & 0.02711 - 0.3152i \\ 0.09054 & -0.1269 - 0.3955i & 0.2058 + 0.1463i & 0.2864 + 0.2213i & 0.4915 + 0.5295i & -0.2566 + 0.1229i & -0.1318 + 0.06502i \\ 0.3998 & 0.1683 - 0.09526i & -0.2707 - 0.3029i & -0.1435 + 0.4721i & 0.2088 - 0.2797i & 0.1282 - 0.04397i & -0.5035 + 0.02425i \end{bmatrix} \tag{8.85}$$

$$M_{4567} = \begin{bmatrix} 0.3749 & 0.3662 & 0.3501 & 0.3584 & 0.2709 & 0.4418 & 0.4535 \\ 0.4918 & -0.2263 - 0.3188i & -0.05239 + 0.1049i & -0.3021 - 0.1664i & 0.05134 - 0.02569i & -0.1856 + 0.5787i & 0.2055 - 0.2405i \\ 0.09054 & 0.3586 + 0.2097i & 0.1473 - 0.2051i & -0.01789 - 0.3615i & -0.7187 + 0.07419i & 0.1132 + 0.261i & -0.145 - 0.02382i \\ 0.3998 & -0.06171 + 0.1833i & -0.3041 + 0.2693i & 0.4521 - 0.1977i & 0.09788 + 0.335i & -0.03915 - 0.1297i & -0.4235 - 0.2733i \end{bmatrix} \tag{8.86}$$

The use of the 7×7 MBS to implement a POVM in dimension 3 or 4 represents an interesting and convenient use of the MCF technology, which could be very interesting in quantum key distribution, quantum state discrimination, and other fields. The particular application at hand will determine which POVM measurement is most useful. We leave further investigations in this direction, including experimental implementation, for future work.

Chapter 9

Conclusions

We have reported the production and the experimental characterization of a High-quality Multiport Beam Splitter ($N \times N$ Beam Splitter) device directly built within a Multicore Fiber. We also report the proposal of the experimental implementation of a PVM and POVM measurement, with up to seven outcomes, utilizing this same device as principal element.

The characterization protocol consisted in estimating the unitary matrix, of complex elements, that represents the operation of the Multiport Beam Splitter over qudits. Each matrix element was formed by two real parameters, the relative phases ϕ_{jk} and the amplitudes u_{jk}. We implemented an interferometic method to measure the relative phases, and used a direct measurement method to measure the amplitudes.

Using a 1550 nm laser and a standard beam splitter we prepared a two-mode state $|\psi_j\rangle \frac{1}{\sqrt{2}} (|1\rangle + e^{i\varphi}|j\rangle)$ and sent it to the the MBS, using demultiplexers to access every core of the MBS. Then we measured in each of the output ports, with detectors, while varing φ. We observed interference patterns of intensity as a function of the modulated phase and applying a fitting function to this curves of interference we obtained some of the relative phases of the matrix. Repeating this process with different two-mode states ($j = 2, ..., N$), we could be able to measure

all the relative phases of the MBS matrix.

To determine the amplitudes we measured the split ratio, sending light from one input port of the MBS and measuring the power at the output ports. this procedure was repeated by sending light from other input ports.

Due to inherent experimental errors, the MBS matrix never was going to be a unitary one. That is why in the last part of our protocol, we applied an optimization method to obtained the nearest unitary matrix to the experimental MBS matrix. By minimizing the infidelity between the experimental matrix $\tilde{U}$ and a real border unitary matrix V.

In the case of the 4×4 MBS, the unitary estimate is almost a symmetric unitary matrix, then, we compared the unitary estimate with the symmetric unitary matrix and obtained a high fidelity of 0.995 ± 0.003. In the case of 7×7 MBS we estimated a unitary matrix, however, it was not symmetric. Though we do not yet have a complete theoretical model, this is what one intuitively expects based on simple considerations concerning the geometry of the cores in the fiber. We note that recent results have shown that even non-symmetric N-port beam splitter devices can serve as primitives for construction of a universal device that implements any $N \times N$ unitary. We also compared the experimental matrix and the unitary estimate and obtained a high fidelity 0.992 ± 0.008.

In the case of both Multiport Beam Splitters, proposed in this thesis, there is a much shorter optical depth, since it is only a large beam splitter, in which the "light splitting process" occurs by a tunneling effect. Then, the propagation losses in the MBS's are reduced. On the other hand, if we had to use the standard model of Reck et al to manufacture the multiport devices, where the number of beam splitter used in given by $N(N-1)/2$, we would need a big number of beam splitters to simulate ours, which would clearly imply a much longer optical depth. However, the Multiport Beam Splitter is not capable of implementing an arbitrary

unit transformation, at least for the dimensions $d = 4$ and $d = 7$, while the Reck configuration can do it, being a universal configuration.

This study is the first step towards future quantum information processing experiments using multicore fiber technology. That is why we wanted to start studying the most direct application that this has, POVM measurements.

Using our setup and based on the Naimark's theorem, we proposed the experimental implementation of a POVM measurements taking into account that we can experimentally modify the phase on each input core of the system. We could achive that by adding different local phases to a d_s sub-set of input cores of the 7×7 MBS, considered as the principal system. The remaining d_a cores was considered as the ancilla system. Where $d_S < d = 7$, with d is the total number of input cores of the MBS. Given by the combinatorial of the cores, we obtained different POVMs that we can implement with our device. This will open the way to its use in a wide variety of applications including quantum tomography and quantum Cryptography.

Appendix A

Measurement to determine demux loss

To characterice a demux we iluminated the core 1 of the demux, with a 1550 nm beam of power equal to $P_a = 17.69$ mW, from left to right as indicated in the Fig.A.1. Then we measured the power P_b, with $b = 1, ..., 7$, and repeated this procedure sending light from other input cores. Finally, we determined the demux's transmissions, t_b, for every core of the demux, which were registered in the Tabla A.1. This gives the following average transmissions:

$$\langle t_{demux1} \rangle = 0.85 \pm 0.15 \ , \tag{A.1}$$

$$\langle t_{demux2} \rangle = 0.90 \pm 0.03 \ . \tag{A.2}$$

demux $\setminus$ P_b	P_1	P_2	P_3	P_4	P_5	P_6	P_7
demux1	9.14	16.44	17.06	15.49	15.24	15.56	14.52
demux2	15.45	15.45	14.93	14.38	15.85	15.74	14.86
demux $\setminus$ t_b	t_1	t_2	t_3	t_4	t_5	t_6	t_7
demux1	0.52	0.94	0.98	0.89	0.87	0.89	0.83
demux2	0.91	0.91	0.88	0.85	0.94	0.93	0.88

Table A.1: Measurement values and determination of demux's transmission. P_b, with $b = 1, ...7$: the output power measured on the demux of the Fig.A.1; t_b: the transmission in each core.

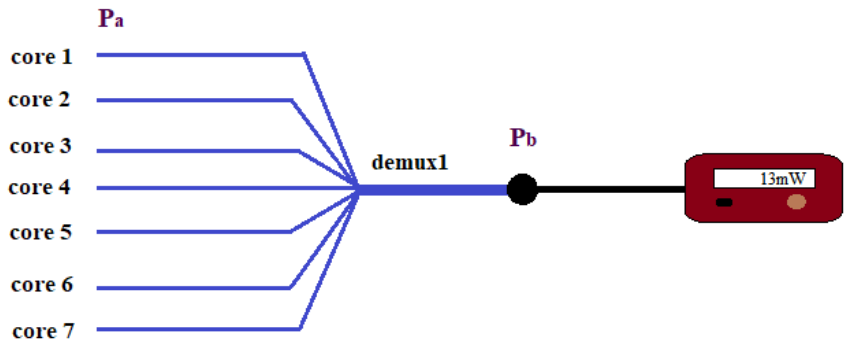

Figure A.1: Scheme to determine the demux's loss: demux1(2): MCF spatial demultiplexers; P_a: input power; P_b, with $b = 1, ..., 7$, the output power measured on the demux

References

[1] M. Reck, A. Zeilinger, H. J. Bernstein, and P. Bertani, "Experimental realization of any discrete unitary operator," *Physical Review Letters*, 1994. 1, 16

[2] W. R. Clements, P. C. Humphreys, B. J. Metcalf, W. S. Kolthammer, and I. A. Walsmley, "Optimal design for universal multiport interferometers," *Optica*, 2016. 1, 16

[3] J. Mower, N. C. Harris, G. R. Steinbrecher, Y. Lahini, and D. Englund, "High-fidelity quantum state evolution in imperfect photonic integrated circuits," *Physical Review A - Atomic, Molecular, and Optical Physics*, 2015. 1

[4] F. Flamini, N. Spagnolo, N. Viggianiello, A. Crespi, R. Osellame, and F. Sciarrino, "Benchmarking integrated linear-optical architectures for quantum information processing," *Scientific Reports*, 2017. 1

[5] S. Rahimi-Keshari, A. Scherer, A. Mann, A. T. Rezakhani, A. I. Lvovsky, and B. C. Sanders, "Quantum process tomography with coherent states," *New Journal of Physics*, 2011. 1

[6] A. Shabani, R. L. Kosut, M. Mohseni, H. Rabitz, M. A. Broome, M. P. Almeida, A. Fedrizzi, and A. G. White, "Efficient measurement of quantum dynamics via compressive sensing," *Physical Review Letters*, 2011. 1

[7] A. Peruzzo, A. Laing, A. Politi, T. Rudolph, and J. L. O'Brien, "Multimode quantum interference of photons in multiport integrated devices," *Nature Communications*, 2011. 1

[8] G. D. VanWiggeren and D. M. Baney, "Swept-wavelength interferometric analysis of multiport components," *IEEE Photonics Technology Letters*, 2003. 1

[9] L. Gan, R. Wang, D. Liu, L. Duan, S. Liu, S. Fu, B. Li, Z. Feng, H. Wei, W. Tong, P. Shum, and M. Tang, "Spatial-division multiplexed Mach-Zehnder interferometers in heterogeneous multicore fiber for multiparameter measurement," *IEEE Photonics Journal*, 2016. 2, 19, 20

[10] S. Rahimi-Keshari, M. A. Broome, R. Fickler, A. Fedrizzi, T. C. Ralph, and A. G. White, "Direct characterization of linear-optical networks," *Optics Express*, 2013. 2, 28, 30

[11] D. J. Richardson, J. M. Fini, and L. E. Nelson, "Space-division multiplexing in optical fibres," 2013. 2, 18

[12] J. Cariñe, G. Cañas, P. Skrzypczyk, I. Šupić, N. Guerrero, T. Garcia, L. Pereira, M. Prosser, G. Xavier, A. Delgado, *et al.*, "Multi-port beamsplitters based on multi-core optical fibers for high-dimensional quantum information," *arXiv preprint arXiv:2001.11056*, 2020. 3

[13] G. A. Steudle, S. Knauer, U. Herzog, E. Stock, V. A. Haisler, D. Bimberg, and O. Benson, "Experimental optimal maximum-confidence discrimination and optimal unambiguous discrimination of two mixed single-photon states," *Physical Review A - Atomic, Molecular, and Optical Physics*, 2011. 3

[14] A. Bisio, G. Chiribella, G. M. D'Ariano, S. Facchini, and P. Perinotti, "Optimal quantum tomography of states, measurements, and transformations," *Physical Review Letters*, 2009. 3

[15] C. C. W. Lim, C. Portmann, M. Tomamichel, R. Renner, and N. Gisin, "Device-independent quantum key distribution with local bell test," *Physical Review X*, 2014. 3

[16] A. K. Ekert, B. Huttner, G. M. Palma, and A. Peres, "Eavesdropping on quantum-cryptographical systems," *Physical Review A*, 1994. 3

[17] A. Peres and D. R. Terno, "Optimal distinction between non-orthogonal quantum states," *Journal of Physics A: Mathematical and General*, vol. 31, pp. 7105–7111, aug 1998. 3, 30

[18] J. B. Brask, A. Martin, W. Esposito, R. Houlmann, J. Bowles, H. Zbinden, and N. Brunner, "Megahertz-Rate Semi-Device-Independent Quantum Random Number Generators Based on Unambiguous State Discrimination," *Physical Review Applied*, 2017. 3

[19] M. a. Nielsen and I. L. Chuang, *Quantum Computation and Quantum Information: 10th Anniversary Edition*. 2011. 6, 8

[20] M. A. Nielsen and I. L. Chuang, *Quantum Computation and Quantum Information: 10th Anniversary Edition*. Cambridge University Press, 2010. 10

[21] S. Pirandola, J. Eisert, C. Weedbrook, A. Furusawa, and S. L. Braunstein, "Advances in quantum teleportation," 2015. 13

[22] A. K. Ekert, "Quantum cryptography based on bell's theorem," *Phys. Rev. Lett.*, vol. 67, pp. 661–663, Aug 1991. 13

[23] E. S. Gómez, S. Gómez, P. González, G. Cañas, J. F. Barra, A. Delgado, G. B. Xavier, A. Cabello, M. Kleinmann, T. Vértesi, and G. Lima, "Device-independent certification of a nonprojective qubit measurement," *Phys. Rev. Lett.*, vol. 117, p. 260401, Dec 2016. 13

[24] B. Yurke, S. L. McCall, and J. R. Klauder, "Su(2) and su(1,1) interferometers," *Phys. Rev. A*, vol. 33, pp. 4033–4054, Jun 1986. 15

[25] S. Danakas and P. K. Aravind, "Analogies between two optical systems (photon beam splitters and laser beams) and two quantum systems (the two-dimensional oscillator and the two-dimensional hydrogen atom)," *Phys. Rev. A*, vol. 45, pp. 1973–1977, Feb 1992. 15

[26] K. Mattle, M. Michler, H. Weinfurter, A. Zeilinger, and M. Zukowski, "Non-classical statistics at multiport beam splitters," *Applied Physics B: Lasers and Optics*, 1995. 17

[27] P. Törmä, I. Jex, and S. Stenholm, "Beam splitter realizations of totally symmetric mode couplers," *Journal of Modern Optics*, 1996. 17

[28] B. J. Metcalf, N. Thomas-Peter, J. B. Spring, D. Kundys, M. A. Broome, P. C. Humphreys, X. M. Jin, M. Barbieri, W. Steven Kolthammer, J. C. Gates, B. J. Smith, N. K. Langford, P. G. Smith, and I. A. Walmsley, "Multiphoton quantum interference in a multiport integrated photonic device," *Nature Communications*, 2013. 17

[29] S. Inao, T. Sato, S. Sentsui, T. Kuroha, and Y. Nishimura, "Multicore optical fiber," 2014. 18

[30] P. Sillard, M. Bigot-Astruc, and D. Molin, "Few-mode fibers for mode-division-multiplexed systems," *Journal of Lightwave Technology*, 2014. 18

[31] L. Zhu, G. Zhu, A. Wang, L. Wang, J. Ai, S. Chen, C. Du, J. Liu, S. Yu, and J. Wang, "18 km low-crosstalk OAM + WDM transmission with 224 individual channels enabled by a ring-core fiber with large high-order mode group separation," *Optics Letters*, 2018. 18

[32] N. Gisin, G. Ribordy, W. Tittel, and H. Zbinden, "Quantum cryptography," *Rev. Mod. Phys.*, vol. 74, pp. 145–195, Mar 2002. 19

[33] S. Pirandola, U. Andersen, L. Banchi, M. Berta, D. Bunandar, R. Colbeck, D. Englund, T. Gehring, C. Lupo, C. Ottaviani, J. Pereira, M. Razavi, J. Shaari, M. Tomamichel, V. Usenko, G. Vallone, P. Villoresi, and P. Wallden, "Advances in quantum cryptography," *arXiv*, 2019. 19

[34] G. B. Xavier and G. Lima, "Quantum information processing with space-division multiplexing optical fibres," 2020. 19

[35] J. F. Dynes, S. J. Kindness, S. W.-B. Tam, A. Plews, A. W. Sharpe, M. Lucamarini, B. Fröhlich, Z. L. Yuan, R. V. Penty, and A. J. Shields, "Quantum key distribution over multicore fiber," *Optics Express*, 2016. 19

[36] R. Lin, A. Udalcovs, O. Ozolins, X. Pang, L. Gan, L. Shen, M. Tang, S. Fu, S. Popov, C. Yang, W. Tong, D. Liu, T. F. Da Silva, G. B. Xavier, and J. Chen, "Telecom Compatibility Validation of Quantum Key Distribution Co-Existing with 112 Gbps/λ/core Data Transmission in Non-Trench and Trench-Assistant Multicore Fibers," in *European Conference on Optical Communication, ECOC*, 2018. 19

[37] T. A. Eriksson, B. J. Puttnam, G. Rademacher, R. S. Luís, M. Takeoka, Y. Awaji, M. Sasaki, and N. Wada, "Inter-Core Crosstalk Impact of Classical Channels on CV-QKD in Multicore Fiber Transmission," in *2019 Optical*

Fiber Communications Conference and Exhibition, OFC 2019 - Proceedings, 2019. 19

[38] G. Cañas, N. Vera, J. Cariñe, P. González, J. Cardenas, P. W. Connolly, A. Przysiezna, E. S. Gómez, M. Figueroa, G. Vallone, P. Villoresi, T. F. Da Silva, G. B. Xavier, and G. Lima, "High-dimensional decoy-state quantum key distribution over multicore telecommunication fibers," *Physical Review A*, 2017. 19, 20

[39] Y. Ding, D. Bacco, K. Dalgaard, X. Cai, X. Zhou, K. Rottwitt, and L. K. Oxenløwe, "High-dimensional quantum key distribution based on multicore fiber using silicon photonic integrated circuits," *npj Quantum Information*, 2017. 19

[40] H. J. Lee, S. K. Choi, and H. S. Park, "Experimental Demonstration of Four-Dimensional Photonic Spatial Entanglement between Multi-core Optical Fibres," *Scientific Reports*, 2017. 19

[41] H. J. Lee and H. S. Park, "Generation and measurement of arbitrary four-dimensional spatial entanglement between photons in multicore fibers," *Photonics Research*, 2019. 19

[42] L. Cui, J. Su, and X. Li, "Distribution of entangled photon pairs over few mode fibers," in *Optics InfoBase Conference Papers*, 2014. 19

[43] A. Sit, R. Fickler, F. Alsaiari, F. Bouchard, H. Larocque, P. Gregg, L. Yan, R. W. Boyd, S. Ramachandran, and E. Karimi, "Quantum cryptography with structured photons through a vortex fiber," *Optics Letters*, 2018. 19

[44] H. Cao, S.-C. Gao, C. Zhang, J. Wang, D.-Y. He, B.-H. Liu, Z.-W. Zhou, Y.-J. Chen, Z.-H. Li, S.-Y. Yu, J. Romero, Y.-F. Huang, C.-F. Li, and G.-C. Guo,

"Distribution of high-dimensional orbital angular momentum entanglement at telecom wavelength over 1km of optical fibre," 2018. 19

[45] D. Cozzolino, E. Polino, M. Valeri, G. Carvacho, D. Bacco, N. Spagnolo, L. K. Oxenløwe, and F. Sciarrino, "Air-core fiber distribution of hybrid vector vortex-polarization entangled states," *Advanced Photonics*, 2019. 19

[46] J. Liu, I. Nape, Q. Wang, A. Vall'es, J. Wang, and A. Forbes, "Multi-dimensional entanglement transport through single-mode fibre," 2019. 19

[47] Z. Zhao, M. Tang, S. Fu, S. Liu, H. Wei, Y. Cheng, W. Tong, P. P. Shum, and D. Liu, "All-solid multi-core fiber-based multipath Mach-Zehnder interferometer for temperature sensing," *Applied Physics B: Lasers and Optics*, 2013. 19

[48] J. E. Antonio-Lopez, Z. S. Eznaveh, P. LiKamWa, A. Schülzgen, and R. Amezcua-Correa, "Multicore fiber sensor for high-temperature applications up to 1000C," *Optics Letters*, 2014. 19

[49] S. Zhou, B. Huang, and X. Shu, "A multi-core fiber based interferometer for high temperature sensing," *Measurement Science and Technology*, vol. 28, p. 045107, feb 2017. 19

[50] H. J. Bernstein, " Must quantum theory assume unrestricted superposition? ," *Journal of Mathematical Physics*, vol. 15, no. 10, pp. 1677–1679, 1974. 25

[51] A. Peres, "Construction of unitary matrices from observable transition probabilities," *Nuclear Physics B (Proceedings Supplements)*, 1989. 30

[52] C. H. Baldwin, A. Kalev, and I. H. Deutsch, "Quantum process tomography of unitary and near-unitary maps," *Physical Review A - Atomic, Molecular, and Optical Physics*, 2014. 33

[53] A. Acín, "Statistical distinguishability between unitary operations," *Physical Review Letters*, 2001. 33

[54] O. Shimakawa, H. Arao, M. Shiozaki, T. Sano, and A. Inoue, "Connector type fan-out device for multi-core fiber," *SEI Technical Review*, 2013. 40

[55] M. Yu Saygin, I. V. Kondratyev, I. V. Dyakonov, S. A. Mironov, S. S. Straupe, and S. P. Kulik, "Robust Architecture for Programmable Universal Unitaries," *Physical Review Letters*, 2020. 47

[56] G. N. M. Tabia, "Experimental scheme for qubit and qutrit symmetric informationally complete positive operator-valued measurements using multiport devices," *Physical Review A - Atomic, Molecular, and Optical Physics*, 2012. 60

[57] J. Shang, A. Asadian, H. Zhu, and O. Gühne, "Enhanced entanglement criterion via symmetric informationally complete measurements," *Physical Review A*, 2018.

[58] N. Bozinovic, Y. Yue, Y. Ren, M. Tur, P. Kristensen, H. Huang, A. E. Willner, and S. Ramachandran, "Terabit-scale orbital angular momentum mode division multiplexing in fibers," *Science*, 2013.

[59] P. Gregg, P. Kristensen, and S. Ramachandran, "Conservation of orbital angular momentum in air-core optical fibers," *Optica*, 2015.

[60] J. Carolan, C. Harrold, C. Sparrow, E. Martín-López, N. J. Russell, J. W. Silverstone, P. J. Shadbolt, N. Matsuda, M. Oguma, M. Itoh, G. D. Marshall, M. G. Thompson, J. C. Matthews, T. Hashimoto, J. L. O'Brien, and A. Laing, "Universal linear optics," *Science*, 2015.

[61] C. Taballione, T. A. W. Wolterink, J. Lugani, A. Eckstein, B. A. Bell, R. Grootjans, I. Visscher, D. Geskus, C. G. H. Roeloffzen, J. J. Renema, I. A. Walmsley, P. W. H. Pinkse, and K.-J. Boller, "88 reconfigurable quantum photonic processor based on silicon nitride waveguides," *Optics Express*, 2019.

[62] J. Cariñe, G. Cañas, P. Skrzypczyk, I. Šupić, N. Guerrero, T. Garcia, L. Pereira, M. A. S. Prosser, G. B. Xavier, A. Delgado, S. P. Walborn, D. Cavalcanti, and G. Lima, "Multi-port beamsplitters based on multi-core optical fibers for high-dimensional quantum information," jan 2020.

[63] H. J. Bernstein, " Must quantum theory assume unrestricted superposition? ," *Journal of Mathematical Physics*, 1974.

[64] A. Peres, "Construction of unitary matrices from observable transition probabilities," *Nuclear Physics B (Proceedings Supplements)*, 1989.